Endothelial sphingosine-1-phosphate receptor 1 deficiency exacerbates brain injury and blood brain barrier dysfunction upon subarachnoid hemorrhage in mice.

Akira Ito[1,4,#], Hiroki Uchida[1,#], Gab Seok Kim[1,&], Giuseppe Faraco[2], Richard Proia[3], Kuniyasu Niizuma[4-6], Teiji Tominaga[4], Josef Anrather[2], Costantino Iadecola[2], Michael J Kluk[1] and Teresa Sanchez[1,2,*].

[1]Department of Pathology and Laboratory Medicine, Center for Vascular Biology, Weill Cornell Medicine, New York, NY

[2]Feil Family Brain and Mind Research Institute, Weill Cornell Medicine, New York, NY.

[3]Genetics of Development and Disease Branch, NIDK, NIH, Bethesda, MD.

[4]Department of Neurosurgery, Tohoku University Graduate School of Medicine, Sendai, Japan

[5] Department of Neurosurgical Engineering and Translational Neuroscience, Graduate School of Biomedical Engineering, Tohoku University, Sendai, Japan

[6] Department of Neurosurgical Engineering and Translational Neuroscience, Tohoku University Graduate School of Medicine, Sendai, Japan

# Equal contributions

& Current address: Department of Neurology, UTHealth, McGovern Medical School, Houston TX.

* Correspondence to: Teresa Sanchez, PhD. Department of Pathology and Laboratory Medicine, Center for Vascular Biology and Feil Familiy Brain and Mind Research Institute, Weill Cornell Medicine, 1300 York Ave, A607B, New York, NY 10065.

ABSTRACT

Blood brain barrier (BBB) dysfunction upon ischemia and hypoxia has been implicated in the exacerbation of neuronal injury in stroke. Despite the therapeutic potential of the cerebrovascular endothelium, the limited understanding of the endothelial signaling pathways governing BBB function restricts progress towards developing novel therapeutic approaches specifically targeting the endothelium. Sphingosine-1-phosphate (S1P) is a potent modulator of endothelial function via its receptors (S1PR). Recent human and mouse studies indicate that vasoprotective endothelial S1P signaling via S1PR1 may be impaired in cardiovascular and inflammatory diseases. Herein, we investigated the expression of S1PR1 in the mouse and human cerebrovascular endothelium and the role of endothelial-specific S1PR1 signaling in brain injury in a mouse model of aneurysmal subarachnoid hemorrhage (SAH), the most devastating type of stroke. We found that S1PR1 is the most abundant S1PR transcript in the mouse brain and in mouse and human brain endothelial cells (20-100 mRNA copies per cell). S1PR1 transcripts were significantly enriched (~6 fold) in mouse cortical microvessels compared to total brain. Using the S1PR1-eGFP knock in mouse, we found that S1PR1-eGFP is abundantly expressed in the cerebrovascular endothelium in the mouse brain. A similar pattern of expression was observed in human brain samples. Endothelial specific deletion of S1PR1 in adult mice (*S1pr1* $^{flox/flox}$ *x Cdh5-Cre*^{ERT2}, referred to as *S1pr1*^{iECKO}), resulted in exacerbation of brain edema, neuronal injury and worsened neurological outcomes upon SAH compared to *S1pr1* $^{flox/flox}$ littermates. No differences in the subarachnoid blood, hemostasis or cerebral blood flow changes during and after SAH were found between groups. Mechanistically, *S1pr1*^{iECKO} exhibited aggravated BBB dysfunction and increased phosphorylation of myosin light chain (MLC) in isolated cortical microvessels, a downstream effector of the Rho-ROCK pathway implicated in endothelial inflammation and barrier dysfunction. Taken together, our data indicate that S1PR1 is an endogenous protective signaling pathway in the endothelium, critical to maintain BBB function and to mitigate neuronal injury in pathological conditions. Thus, the therapeutic and diagnostic potential of the endothelial sphingosine-1-phosphate pathway in stroke deserves further study.

INTRODUCTION

Despite decades of intensive research, stroke is still a leading cause of mortality and long-term disability worldwide [1] and novel therapeutic strategies are need. The cerebrovascular endothelium, in coordination with pericytes [2, 3] and astrocytes [4] plays a critical role in the maintenance of the blood brain barrier (BBB). BBB dysfunction has been implicated in the exacerbation of neurovascular ischemic, hypoxic and inflammatory injury in stroke. For instance, the use and effectiveness of current therapies for ischemic stroke (i.e. tissue plasminogen activator, tPA, or mechanical recanalization) are severely limited by the vascular complications of reperfusion injury (i.e. blood brain barrier dysfunction leading to vasogenic edema and hemorrhagic transformation)[5-9]. In hemorrhagic stroke, perihematoma edema and volume expansion is associated with worsened outcomes [10]. In subarachnoid hemorrhage (SAH), blood brain barrier breakdown occurs in the acute phase and correlates with more severe neurological deficits [11-13]. Although the therapeutic potential of the cerebrovascular endothelium is beginning to be recognized [14-17], *the limited understanding of the endothelial signaling pathways governing BBB function/dysfunction in pathological conditions, restricts progress towards developing novel endothelial-targeted therapies.*

S1P, a bioactive lipid very abundant in plasma, is a potent modulator of endothelial and lymphocyte function. Plasma S1P originates from endothelial cells[18, 19] and erythrocytes[20] and it is bound to lipoproteins (e.g. HDL[21, 22] via apolipoprotein M (ApoM)[22], albumin and other chaperones. In mice, S1P signaling via S1PR1 is required for embryonic and postnatal vascular development and maturation in brain and other organs [23, 24] [25]. In adult mice, S1PR1 promotes endothelial barrier function, vascular stabilization and inhibits endothelial inflammation [26-28]. These effects are dependent on the activation of anti-inflammatory signaling pathways (Gi-

phosphatidylinositol-3-kinase leading to activation of Rac and Akt) which strengthen endothelial barrier function by promoting actin cytoskeleton dynamics (cortical actin assembly) and adherens junctions assembly to the cytoskeleton. In contrast, S1P binding to S1PR2 induces barrier dysfunction and activates pro-inflammatory signaling pathways (e.g. NFκB) in a Rho-Rho kinase dependent way. S1P-S1PR1 antiinflammatory signaling pathway is predominant in the endothelium when S1P is bound to HDL via ApoM [28] (Reviewed in [17]). Indeed, a good part of the cardiovascular protective effects of HDL depend on its content of S1P [29-31] and ApoM [28], which also has been shown to protect plasma S1P from degradation [22]. Recent studies indicate that S1P anti-inflammatory and vasoprotective signaling via S1PR1 could be limiting in human cardiovascular and inflammatory diseases [31-34] [17]. For instance, in coronary artery disease, the content of ApoM or S1P in the HDL fraction is significantly reduced, and it inversely correlates with the severity of the disease[31, 32]. In addition, in patients suffering inflammatory conditions such diabetes or sepsis, plasma ApoM levels are significantly decreased compared to control patients [35, 36].

Interestingly, S1PR1 also plays a critical role in lymphocyte trafficking and function: mice lacking S1PR1 in hematopoietic cells are lymphopenic due to impaired egress from thymus and lymphoid organs [37]. Indeed, the immunosupressors, Fingolimod (FTY720) [38, 39], and Siponimod (BAF312)[40], which have been approved by the FDA for multiple sclerosis are potent S1PR1 agonists. Given the phenotype of the mice lacking S1PR1 in hematopoietic cells[37] and *in vitro* studies which indicate that FTY720-P induces desensitization of S1PR1 [41, 42], it is accepted that Fingolimod, Siponimod and other agonists [43] and antagonists [44] of S1PR1 lead to immunosuppression via inhibition of S1PR1 signaling in lymphocytes.

Recent studies attempting to understand the role of S1P in cerebral ischemia have relied on the use of these pharmacological modulators of S1PR1 [45, 46], [47] [48], which

protected in experimental stroke. Although the mechanisms are not completely clear, FTY720 protection has been attributed to its immunosuppressive effects [48] and its ability to desensitize S1PR1 (reviewed in [17]). *Thus, these studies could not determine the role of endothelial-specific S1P signaling in BBB function modulation and its impact on brain injury and stroke outcomes.* Although immunosuppression is protective in experimental stroke, it is not clear that it could be a good therapeutic strategy in humans, since it also increases the vulnerability of patients to infections [49, 50], a leading cause of mortality in stroke patients[51, 52]. Nevertheless, Fingolimod [53-55] and Siponimod are currently being tested in stroke clinical trials. *Understanding the role of endothelial S1P signaling in stroke will be pivotal for future design of novel vasoprotective therapeutic agents targeting this pathway specifically in the endothelium without compromising the immune response.*

In order to bridge this knowledge gap and given the pathophysiological relevance of the S1P-S1PR1 pathway in humans, in this study we aimed to investigate the expression of S1PR1 in the mouse and human cerebrovascular endothelium as well as the role of endothelial-specific S1PR1 signaling in modulation of blood brain barrier function and its impact on brain injury upon subarachnoid hemorrhage, the most devastating type of stroke. Our results show that S1PR1 is an endogenous protective signaling pathway in the endothelium, critical to maintain BBB function and to mitigate neuronal injury in SAH. They also highlight the critical role of the endothelial S1PR1 pathway in the pathophysiology of cerebral hypoxia-ischemia as well as its therapeutic potential.

METHODS

Mice. All animal experiments were approved by the Weill Cornell Institutional Animal Care and Use Committee. Endothelial cell specific *S1pr1* knockout mice (*S1pr1*$^{flox/flox}$*xCdh5–Cre*^{ERT2}*;* referred to as *S1pr1*^{iECKO}) were generated as we have described [56]. *S1pr1*$^{flox/flox}$ mice [24] were crossed to *Cdh5–Cre*^{ERT2} mice [57] to

generate *S1pr1*$^{flox/flox}$ *Cdh5-Cre*^{ERT2} mice. Mice were treated with tamoxifen (Sigma-Aldrich) by oral gavage (75 mg kg^{-1}) for 3 days at the age of 8 weeks and used for the experiments 3-4 weeks after tamoxifen treatment. *S1pr1*$^{flox/flox}$ littermates treated with tamoxifen were used as control mice. S1pr1-eGFP knock in mice [58] weighing 26-30 g were used for the expression studies. All experiments were performed in male mice.

Isolation of cortical microvessels. The brain microvessels were isolated as we have previously described [59]. All procedures were performed in a cold room. The brains were collected and rinsed in MCDB131 medium (Thermo Fisher Scientific) with 0.5% fatty acid-free BSA (Millipore Sigma). The leptomeninges, cerebellum, brainstem and white matter were removed on ice. Ipsilateral cortices were homogenized in 8 mL of MCDB131 medium with 0.5% fatty acid-free BSA using a 7-mL loose-fit Dounce tissue grinder (Sigma-Aldrich) with 10 strokes. The homogenates were centrifuged at 2,000 g for 5 min at 4 °C. The pellet was suspended in 15% dextran (molecular weight ~70,000 Da, Sigma-Aldrich) in PBS and centrifuged at 10,000 g for 15 min at 4 °C. The pellet was resuspended in MCDB131 with 0.5% fatty acid-free BSA and centrifuged at 5,000 g for 10 min at 4 °C. The pellet contained the brain microvessels.

Isolation of mouse primary neurons and mouse mixed glial cells.

Mouse (C57BL6) E16.5 embryos were used for primary cortical neuron isolation as we previously described [60]. Cortices were collected and incubated with 0.25% trypsin for 15 min at 37 °C for tissue digestion. Fetal bovine serum was added to stop the trypsin activity. After centrifugation, the supernatant was discarded and DMEM complete media containing 10% FBS and antibiotics were added to the cells. The cell suspension was passed through 70 µm cell strainer (BD Biosciences, Falcon) and was plated on poly-L-lysine (Sigma Aldrich, St Louis, MO) coated dishes with DMEM complete media. The next day, the medium was changed to Neurobasal media containing B27 supplement, antibiotics and GlutaMAX (Life Technologies). At 7 days *in vitro*, the cells (>95% NeuN

positive) were harvested for RNA isolation and gene expression quantification by reverse transcription and quantitative PCR (RT-qPCR).

Mixed glial cell culture was prepared using the mouse brains from postnatal day 2 mouse as we previously described [60] Briefly, cerebral cortices were dissected, trypsinized with of 0.25% trypsin–EDTA in Hank's Balance Salt Solution (HBSS) and were incubated with trypsin (Thermo scientific) and DNase (Worthington) for 15 min at 37 °C. Foetal bovine serum was added to the cell suspension to stop trypsin digestion. Cell suspension was centrifuged and the pellet was resuspended with DMEM containing 20% FBS and antibiotics. Cell suspension was filtered with a 100-µm cell strainer (BD Falcon) into another 50 ml conical tube. Cells were plated onto six-well plates, which were pre-coated with poly-D-lysine. Three days after plating, the media was changed to DMEM containing 10% FBS and antibiotics. Cells were maintained in DMEM containing 10% FBS and antibiotics at 37 °C with 5% CO2, with a medium change every 3 days. At day 10 after plating RNA was isolated for determination of gene expression by RT-qPCR.

Endovascular perforation SAH surgery. SAH surgery was performed on C57/BL6/J, *S1pr1*^{iECKO} mice and their littermate *S1pr1*$^{flox/flox}$ controls as we have previously described [61]. In brief, surgery was performed using a dissecting surgical microscope. Temperature was maintained at 36.5–37.5 °C by using a thermostatic blanket (Harvard Apparatus, CMA 450 Animal Temperature Controller) throughout the procedure. Mice were anesthetized with isoflurane inhalation delivered by facemask with O_2. A 15 mm midline vertical incision was made on the skin in the head. The head was fixed in stereotactic frame and cerebral blood flow was measured by Laser-speckle imager (PeriCam PSI system, Perimed, Sweden). During surgery, mice were in supine position. A 10 mm midline vertical incision was made on the skin in the neck. The common carotid, external carotid and internal arteries were dissected from the adjacent tissue.

The superior thyroid artery and the occipital artery were cauterized and cut. The external carotid artery was sutured with a dead knot and cauterized above the suture. A second suture loop was also placed in the external carotid artery just before the bifurcation of the common carotid artery. A slit-knot was placed around the common carotid artery. A small clip was applied to the internal carotid artery and the slip-knot around the common carotid artery was tightened temporally. A small incision was made in the external carotid artery stump. A 5-0 monofilament with a modified tip (0.3 mm x 0.3 mm or 0.3 mm x 1.7 mm) was inserted into the incision and the knot around the external carotid artery was tightened to prevent bleeding. Then, the monofilament was advanced to the common carotid artery, the small clip on the internal carotid artery was removed and the monofilament was guided through the external carotid artery to the internal carotid artery. The knot around the common carotid artery was opened again and the monofilament was introduced to the bifurcation of the internal carotid artery. The monofilament was gently pushed ~1 mm further and then withdrawn to the external carotid artery. The knot around the external carotid artery was loosen and the monofilament was slowly removed. The external carotid artery was quickly ligated to prevent bleeding. The mouse was turned in prone position and induction of subarachnoid hemorrhage was confirmed by reduction of cerebral blood flow by Laser-speckle contrast imager. After the surgery, all animals were maintained in a small animal heated recovery chamber. Two different severities of SAH models were created by changing the tip shapes of a 5-0 monofilament: a rounded tip 0.3mm (width) x 0.3 mm (length) was used for mild SAH model or a tip 0.3 mm (width) x 1.7 mm (length) for severe SAH model. The surgeon and the investigator conducting the analysis were blinded to the genotype of the mice. Animals which did not exhibit a reduction in CBF upon endovascular rupture were excluded from the study.

RNA isolation, reverse transcription and quantitative PCR analysis (RT-qPCR)

Total RNA from mouse brain, cells and microvessels was prepared using RNeasy Mini Kit (Qiagen, Valencia, CA) as instructed by the manufacturer. To generate cDNA, 100 ng of RNA was reverse transcribed using random primers and SuperScript II RT-polymerase (Invitrogen, Carlsbad, CA). Primers were designed using the Primer Express oligo design program software (Applied Biosystems, Foster City, CA). Real-time quantitative PCR was performed using the SYBR Green I assay on the ABI 7500 Sequence Detection System (Applied Biosystems)**.** PCR reactions for each cDNA sample were performed in duplicate and copy numbers were calculated using standard curves generated from a master template as we previously described. The sequence of the primers used for qPCR are shown in Table 2.

S1PR1 Immunohistochemistry

Human tissues were retrieved from Brigham and Women's Department of Pathology archives; this work was approved by the Institutional Review Board (Protocol #2013P001431).

Immunohistochemistry for S1PR1 was performed on an automated stainer (Leica Bond III, Leica Biosystems, Buffalo Grove, IL) using an anti-human S1PR1 rabbit polyclonal antibody (Santa Cruz Biotechnology Inc.) at a final concentration of 1.3 ug/ml. The IHC technique for S1PR1 was validated as we have previously described [62]. 5µm formalin fixed paraffin embedded tissue sections of human frontal cortex were deparaffinized and processed using heat induced epitope retrieval with an EDTA-based buffer (Leica #AR9640) for 20 minutes and incubated with primary antibody for 30 minutes at room temperature. Secondary antibody (polymer) incubation (10 minutes) and diaminobenzidine-based signal generation (10 minutes) were performed per manufacturer's instructions (Leica # DS9800). Pictures were taken using SPOT Insight Gigabit camera and SPOT Imaging Software (5.1).

Immunofluorescence staining

Under deep anesthesia, mice were perfused with cold PBS and subsequently with 4% PFA in PBS solution. The brains were removed, postfixed with 4% PFA for 24 h, transferred to 30% sucrose solution in PBS, embedded in OCT media and frozen. Coronal sections were cut (9 µm) in a cryostat. Sections were washed three times with PBS and were then blocked with blocking solution (5 % bovine serum albumin, 0.8 % skim milk, and 0.3 % Triton X-100 in TBS) for 1 h and incubated with the specified primary antibodies in blocking solution overnight on a shaker at 4 °C, followed by the appropriate secondary antibodies and 4',6-diamidino-2-phenylindole (DAPI) for 1 hours at room temperature and were mounted onto slides. Samples were observed on an FluoView FV10i confocal microscope (Olympus, Japan) (original magnification, x 60).

Protein extraction from brain microvessels and western blotting. Brain microvascular fragments were lysed in HEPES-RIPA buffer (50 mM HEPES pH 7.5; 1% Triton; 0.5% sodium deoxycholate; 0.1% SDS; 500 mM NaCl; 10 mM MgCl2; 50 mM β-glycerophosphate) with 1x Protease inhibitor cocktail (CalBiochem), 1 mM Na3VO4 and 1 mM NaF and centrifuged at 15,000 r min^{-1} for 15 min. Equal amount of proteins were mixed with SDS sample buffer, boiled and separated on a 4-15% polyacrylamide gel (Bio-Rad), transferred to PVDF membranes (Millipore Sigma), and blocked 5 % milk in 0.1% Tween-20 in TBS. Immunoblot analysis was performed with S1PR1 (1:250; Santa Cruz, cat. no. sc25489), p-MLC (1:1000; Cell Signaling, cat. no. 3671), and β-actin (1:1,000; Santa Cruz, cat. no. sc-1616 HRP) antibodies. Membranes were washed with 0.1% Tween-20 in TBS, incubated with anti-rabbit IgG secondary antibody conjugated to horseradish peroxidase (1:2,000; Cell Signaling), and protein bands were visualized with enhanced chemilumescent (ECL) reagent (Thermo Fisher Scientific) on a Protec OPTIMAX X-Ray Film Processor. Relative band intensities were obtained by densitometric analysis of images using ImageJ software.

Brain endothelial cell isolation and assessment of deletion efficiency of endothelial *S1pr1 mRNA*. Two weeks after tamoxifen treatment, mice were sacrificed and the brains were collected and rinsed in MCDB131 medium (Thermo Fisher Scientific) with 0.5% fatty acid-free BSA (Millipore Sigma). The cortices were homogenized in MCDB131 medium using a 7-mL loose-fit Dounce tissue grinder (Sigma-Aldrich) with 15 strokes. The homogenate was mixed with same amount of 30% dextran (molecular weight ~70,000 Da, Sigma-Aldrich) in PBS and centrifuged at 4,500 r min^{-1} for 15 min at 4 °C. The pellet was resuspended in MCD131 medium and centrifuged at 2,400 r min^{-1} for 10 min. The pellet was resuspended in Liberase TM solution (3.5 U; Roche) with DNaseI (0.4 U; AppliChem Inc) and digested at 37.0 °C for 90 min. The enzymatic reaction was stopped by adding 2 mM of EDTA and 2% of BSA. After centrifugation at 2,400 r min^{-1} for 10 min, the pellet was incubated in purified Rat Anti-Mouse CD31antibody (MEC13.3) (1 : 100; BD Biosciences) with Dynabeads Sheep Anti-Rat IgG (Invitrogen, cat. no. 11035) for 35 min. CD31 positive endothelial cells were isolated by using DynaMag-2 Magnet (Thermo Fisher Scientific). Total RNA was extracted from the isolated endothelial cells using shredder (Qiagen) and RNeasy Mini Kit (Qiagen) with RNase-free DNase treatment (Qiagen) according to the manufacturer's instructions. Reverse transcription was carried out using Verso cDNA Synthesis Kit (Thermo Fisher Scientific). Real-time PCR was performed on a real-time PCR system (Applied Biosystems, ABI 7500 Fast) by using PerfeCTa SYBR Green Fast Mix Low ROX. PCR primer sequences for target molecules are in Table 2.

Grading system for SAH. Blood volume in the subarachnoid space was assessed using the grading system previously reported [63]. Mice were sacrificed under deep anesthesia 24 h after SAH induction and the brains were removed. Pictures of ventral surface of the brain depicting the basal cistern with the circle of Willis and the basilar artery were taken using a stereomicroscope (Olympus, SZX16) equipped with digital

camera (Olympus, DP12). The basal cistern was divided into 6 segments and a grade from 0 to 3 was given to each segment: Grade 0, no subarachnoid blood; Grade 1, minimal subarachnoid blood; Grade 2, moderate blood clot with recognizable arteries; Grade 3, blood blot obliterating all arteries. Blood volume was evaluated by a total score ranging from 0 to 18 from six segments.

Tail bleeding assay. Tail bleeding time was determined as described previously[64]. A mouse was anesthetized with a mixture of ketamine and xylazine, and body weight was measured. The mouse was placed on a heating pad in prone position, the tail tip was about 4 cm blow the body horizon. A distal 5 mm segment of the tail was amputated, and the tail was immediately immersed in PBS pre-warmed at 37 °C. The time to complete arrest of bleeding was determined: complete arrest is no blood flow for 1 minute. The blood volume was determined by hemoglobin assay. Blood cells were separated by centrifuge at 4,000 r/min for 5 min at room temperature, and erythrocytes were resuspended in BD Pharm Lyse (BD Biosciences). After 10 min incubation in the buffer, the lysate was centrifuged at 10,000 rpm/min for 5 min. Hemoglobin concentrations were measured spectrophotometrically at 550 nm using a plate reader (Molecular Devices, SpectraMax M2e).

Mortality and neurological outcome. Mortality was assessed at 24, 48 and 72 hours after SAH induction. Gross neurological outcome was blindly evaluated before and at 24, 48 and 72 hours after surgery by sensorimotor scoring as described previously [65, 66]. Briefly, a motor score (0 to 12; spontaneous activity, limb symmetry, climbing, and balance) and a sensory score were used. Gross neurological outcome was evaluated by a total score of 4 to 24. Higher scores indicate better neurological outcome.

Brain water content. Brain edema was determined by using the wet/dry method as previously described [67]. Mice were sacrificed at 72 hours after surgery and the brains were quickly removed and separated into the left and right cerebral hemispheres and

weighed (wet weight). The brain specimens were dried in an oven at 55°C for 72 hours and weighed again (dry weight). The percentage of water content was calculated as ([wet weight-dry weight]/wet weight) x 100%.

Cell death detection. DNA strand breakage during apoptosis after SAH was assessed by phospho-histon H2A.X (Ser 139) immunofluorescence as previously described [68]. Because phosphorylation of histone H2A.X at Ser 139 (γ-H2AX) is abundant, fast, and correlates well with each DNA strand breakage, it is the most sensitive marker that can be used to examine the DNA damage [69, 70]. Mice were deeply anesthetized and perfused with cold PBS and subsequently with 4% PFA in PBS solution. The brains were removed, post-fixed with 4% PFA for 24 h and transferred to 30% sucrose solution. Frozen brains were cut with a 10 µm of thickness by a cryostat (Leica, CM3050 S). The brain slices were blocked with TBS- blocking solution (5% bovine serum albumin and 0.5% Tween 20 in PBS) for 1 hour at room temperature and incubated with phospho-histone H2A.X (Ser 139) (20E3) antibody (1:100; Cell Signaling) in blocking solution overnight on a shaker at 4 °C. Sections were washed three times with 0.5% Tween 20 in PBS and then incubated with goat anti- rabbit IgG Alexa- 488 (1:200; Life Technologies, cat. no. A-11008). DAPI (40 ,6-diamidino-2-phenylindole) staining was used as a counter staining. Sections were imaged by using an FluoView FV10i confocal microscope (Olympus, Japan) (original magnification, x 40). For quantification, the percentage of phospho-histone H2A.X positive cells per DAPI positive cells from three different fields in the ipsilateral cerebral cortex area per mouse (bregma -1.64 to -1.28 mm) were counted and the average values were plotted.

Assessment of blood brain barrier dysfunction.

To assess albumin extravasation, Evans blue dye (EBD) was used because EBD binds to plasma albumin[71]. Mice were anesthetized and 2% EBD (4 ml kg^{-1}) was injected in the external jugular vein 21 hours after surgery. After 3 hours circulation, mice were

343 deeply anesthetized and perfused with cold PBS to remove intravascular dye. The
344 ipsilateral hemispheres were removed and homogenized in 50% trichloroacetic acid in
345 PBS. The lysate was centrifuged at 15,000 rpm min^{-1} twice for 15 min at 4 °C, and the
346 supernatant was used to measure fluorescence (excitation/ emission = 620/680 nm,
347 SpectraMax M2e, Molecular Devices). The relative fluorescence units (R.F.U.) were
348 normalized by the brain weights. To histologically confirm the plasma leakage into the
349 brain parenchyma, 70 kDa dextran-TMR was injected through jugular vein and let
350 circulate for 1h. Brain was removed without perfusion, embedded OCT compound
351 directly and frozen [72]. Sections were cut (9 µm) in a cryostat and fixed with 4% PFA
352 before Immunohistochemistry. After staining with anti Glut-1 antibody, the ipsilateral
353 cortex was observed on an FluoView FV10i confocal microscope (Olympus, Japan)
354 (original magnification, x 60).
355 **Statistical analysis.** All results were expressed as mean ± SEM. Statistical analysis
356 were performed with GraphPad Prism (GraphPad Software, Version 7.0c) by using two-
357 tailed Student's t-test, one-way analysis of variance (ANOVA) followed by Tukey's test or
358 two-way ANOVA followed by Bonferoni's test. *P* values < 0.05 were considered
359 statistically significant.
360

RESULTS

Expression of S1PR1 in the mouse and human brain

We first investigated the expression of S1PR in brain, mouse primary neurons and mouse brain endothelial cells by reverse transcription and quantitative PCR analysis (RT-qPCR), as we have previously described [62, 73]. We found that S1PR1 is robustly expressed, being the most abundant S1PR transcript in the mouse brain *in vivo*, (Fig. 1A, 20.5± 2.4 copies/10^6 18S, which is equivalent to approximately 20.5± 2.4 S1PR1 mRNA copies/cell [74]), as well as in the mouse brain endothelial cell line bEnd.3 [75] (Fig. 1B, 87.3±2.9 copies/cell), mouse primary neurons (Fig. 1C, 16.4±1.3 copies/cell) and mouse primary mixed glial cells (Fig. 1D, 8.3±0.15 copies/cell) *in vitro.* Then, we compared the expression of S1PR1 in cortical microvessels fragments [56] to its expression in total brain. Interestingly, we found that S1PR1 transcripts are highly enriched in cortical microvessels when compared to total brain (Fig. 1E, ~6 fold enrichment in microvessels *vs* whole brain).

Using the S1pr1-eGFP knock in mice, in which S1PR1-eGFP fusion protein is expressed under the control of the endogenous S1PR1 promoter [58], we found that S1PR1 is abundantly expressed in the endothelium of cerebral microvessels throughout the brain (Fig. 2A, B, representative pictures from corpus callosum and cortex) as assessed by detection of S1PR1-eGFP and immunofluorescence (IF) analysis for the glucose transporter 1 (Glut-1).

S1PR1 is also expressed in neurons in various anatomical areas, mainly in the neuropil, as assessed by Nissl and microtubule associated protein (MAP)-2 staining. Representative pictures of cortex and hippocampus are shown (Supplementary Figures 1 and 2, A and B). In white matter areas (e.g. corpus callosum and internal capsule, supplementary figures 1C and 2C, D), S1PR1-eGFP is localized mainly in the neuronal

processes, surrounding MAP2 signal. Only some fibrous astrocytes express S1PR1 (Supplementary Figure 3).

A similar pattern of expression was observed in the mouse brain when immunofluorescence analysis was conducted using a S1PR1 antibody previously validated in our laboratory [62] (data not shown).

In order to investigate the expression of S1PR1 in the human brain, we conducted IHC analysis in sections from the frontal lobe. The S1PR1 antibody and IHC protocol used in human samples were previously validated in our laboratory [62]. Representative pictures of the frontal cortex are shown in Figure 3. S1PR1 immuno positivity was observed both in the grey matter (GM) and subcortical white matter (WM) areas (Figure 3A, low magnification). S1PR1 was widely detected in the cerebrovascular endothelium of parenchymal vessels (in the grey matter and white matter, Fig. 3B, D-F) and pial vessels (Fig. 3C). In the grey matter, S1PR1 staining was observed mainly in the neuropil (Fig. 3B, C). In the subcortical white matter, the detection of S1PR1 was more diffuse and weaker compared to the signal observed in the microvessels (Figure 3E and F).

Altogether, our data indicate that, S1PR1 is the most abundant S1PR transcript in the brain, and in brain endothelial cells, neurons and mixed glial cells *in vitro*. S1PR1 protein is also widely detected in the mouse and human brain, in the cerebrovascular endothelium and the grey matter neuropil. S1PR1 mRNA is highly enriched in mouse cerebral microvessels when compared to total brain.

Endothelial S1PR1 is an endogenous protective pathway induced in cerebral microvessels after SAH

In order to investigate the role of endothelial S1PR1 signaling in the pathophysiology of aneurysmal SAH, we used the endovascular rupture model of SAH[61], which is a well established and reproducible model that recapitulates key features of the pathophysiology of the acute phase of SAH. 24, 48 and 72 hours after SAH, cerebral

412 microvessels were isolated from the mouse cortex of wild type mice to determine
413 sphingosine 1-phosphate receptor 1 (S1PR1) mRNA and protein levels compared to
414 sham mice. We found that S1PR1 mRNA levels in cortical microvessels were
415 significantly increased at 24h after SAH (3.14 ± 0.55 fold induction) compared to sham
416 (Fig. 4A). Gfap mRNA levels in microvessels were significantly higher 24 h after SAH
417 compared to sham (Fig. 4B, 5.14 ± 0.55 fold induction). The levels of endothelial (Tjp-1,
418 Fig. 4C), pericyte (Anpep, CD13, Fig. 4D) or astrocyte end foot (Aqp4, Fig. 4E) markers
419 did not significantly change suggesting similar cell composition among the microvessel
420 preparations from these groups of mice. S1PR1 protein was widely detected by western
421 blot assay in cerebral microvessels in sham animals (Supplementary Figure 4). A
422 modest increase in S1PR1 protein levels at 24 hours after SAH was observed ($1.68 \pm$
423 0.19-fold). These data indicate that, in the acute phase of SAH, neurovascular
424 inflammation occurs. In addition, S1PR1 mRNA and protein levels in cerebral
425 microvessels were significantly increased upon SAH.
426 Given the abundant expression of S1PR1 in the cerebrovascular endothelium in the
427 mouse and human brain, and the enrichment in S1PR1 mRNA in mouse cortical
428 microvessels compared to total brain, we aimed to investigate the role of endothelial
429 S1PR1 signaling in early brain injury (EBI) after SAH. We generated endothelial-specific
430 S1PR1 null mice (S1PR1 ^{iECKO}) by treating adult *S1pr1*$^{flox/flox}$*xCdh5–Cre*^{ERT2} mice (~2
431 month old) with 75 mg kg^{-1} tamoxifen for 3 consecutive days (Fig.4F) as we have
432 recently described[56]. *S1pr1*$^{flox/flox}$ littermate mice were also treated with tamoxifen and
433 used as wild type control. We assessed the efficiency of deletion in S1PR1^{iECKO} by
434 isolating brain endothelial cells from mice 2 weeks after tamoxifen treatment. RT-qPCR
435 analysis demonstrated ~90% reduction of *S1pr1* expression in *S1pr1*^{iECKO} mice
436 compared to *S1pr1*$^{flox/flox}$ littermate mice treated with tamoxifen in the same manner (Fig.
437 4F). We previously reported that, in resting conditions, postnatal endothelial deletion of

S1PR1 does not have an impact on central nervous system vascular development, maturation, or pattern formation [56].

S1pr1^{iECKO} and *S1pr1*$^{flox/flox}$ littermates were subjected to SAH surgery using a modified 5.0 suture (0.3 mm x 1.7 mm) to induce severe SAH as described in the method section [61]. The mortality rates were 10% in *S1pr1*$^{flox/flox}$ mice at day 1, 2 and 3 after SAH. Interestingly, the mortality rates in endothelial-specific S1PR1 null mice (*S1pr1*^{iECKO} , 40% at day 1, and 60% at day 2 and 3, Fig. 4G) were significantly higher compared to wild type (*S1pr1*$^{flox/flox}$,.

Given the high mortality rate in *S1pr1*^{iECKO} subjected to the severe SAH model (Fig. 4G), we used a milder SAH model for subsequent studies, by changing the shape of the tip of the nylon suture to perforate the cerebral artery (0.3 mm x 0.3 mm, as described in methods section). When *S1pr1*^{iECKO} mice were challenged with mild SAH, they exhibited a trend towards a higher mortality rate (26.3% in day 1, 2 and 3) compared to *S1pr1*$^{flox/flox}$, which exhibited a mortality rate of 7.7% at day 1, 2 and 3 (Fig. 4H), although it was not statistically significant. Altogether these data indicate that endothelial-specific deletion of S1PR1 in mice increases mortality in the acute phase of SAH.

Genetic deletion of *S1pr1* in the endothelium has no effect on blood volume in the subarachnoid space, hemostasis or CBF changes after SAH.

The volume of blood in the subarachnoid space, which depends on the amount of bleeding and the clearance, directly correlates with worse outcomes after SAH [76] [63]. Thus, we quantified the amount of subarachnoid blood upon SAH in *S1pr1*$^{flox/flox}$ and *S1pr1*^{iECKO} mice by image analysis using a previously described SAH grading system [63]. No significant differences were observed in the amount of subarachnoid blood between *S1pr1*$^{flox/flox}$ and *S1pr1*^{iECKO} mice 24h after SAH (Fig. 5A, representative pictures). SAH grading was 11.50 ± 0.62 in *S1pr1*$^{flox/flox}$ mice and 11.67 ± 0.42 in *S1pr1*^{iECKO} (Fig. 5B). In addition, we determined the role of endothelial-specific S1PR1

in hemostasis using the tail bleeding assay [64]. We did not find any significant differences in the bleeding times or blood volumes between *S1pr1*$^{flox/flox}$ and *S1pr1*^{iECKO} mice in the tail bleeding assay. Bleeding times were 68.88 ± 4.98 seconds in *S1pr1*$^{flox/flox}$ and 63.8 ± 4.14 seconds in *S1pr1*^{iECKO} (Fig. 5C). Hemoglobin contents, assessed by measuring the absorbance at 550 nm, were 0.73 ± 0.07 in *S1pr1*^{iECKO} mice compared to 0.70 ± 0.12 in *S1pr1*$^{flox/flox}$ mice (Fig. 5D). Altogether, these data indicate that hemostasis is not impaired in *S1pr1*^{iECKO} mice compared to wild type mice and that the amount of blood in the subarachnoid space 24 h upon SAH is similar in wild type and *S1pr1*^{iECKO} *mice.*

We also determined cerebral blood flow (CBF) changes during SAH in both groups of mice by Laser-Speckle flowmetry (Figure 5E). CBF in the middle cerebral artery (MCA) territory rapidly dropped ~1 minute after SAH in a similar way in both *S1pr1*$^{flox/flox}$ and *S1pr1*^{iECKO} mice. In the ipsilateral hemisphere, CBF dropped to 40.26 ± 4.09% of basal in *S1pr1*$^{flox/flox}$ *and* to 31.65 ± 3.46% of basal in *S1pr1*^{iECKO}; in the contralateral hemisphere, CBF dropped to 77.32 ± 3.90% of basal in *S1pr1*$^{flox/flox}$ and to 82.42 ± 3.72% of basal in *S1pr1*^{iECKO}. Afterwards, as shown in Figure 5E, CBF progressively recovered similarly in S*1pr1*$^{flox/flox}$ and *S1pr1*^{iECKO} mice. 2 h after SAH, in the ipsilateral hemisphere, CBF recovered to 82.83 ± 5.88% of basal in *S1pr1*$^{flox/flox}$ *and* to 87.46 ± 7.15% of basal in *S1pr1*^{iECKO}; in the contralateral side CBF recovered to 95.34 ± 4.86% of basal in *S1pr1*$^{flox/flox}$ and to 102.81 ± 1.97% of basal in *S1pr1*^{iECKO}. These data indicate that genetic deletion of *S1pr1* in the endothelium did not have a significant impact in CBF changes upon SAH.

Finally, no significant differences were observed in arterial O_2 saturation, heart rate, pulse distention (a surrogate of pulse pressure) and respiratory rate between *S1pr1*^{iECKO} and *S1pr1*$^{flox/flox}$ mice, before or after SAH (Table 1).

Altogether, these data indicate that endothelial-specific deletion of S1PR1 in adult mice did not have a significant impact on bleeding or clearance of subarachnoid blood, cerebral blood flow changes or systemic physiological parameters such as heart rate, respiratory rate, O_2 saturation or pulse distension.

Endothelial deletion of *S1pr1* exacerbates brain edema and cell death after SAH leading to worsened neurological outcomes.

In order to determine the impact of the lack of endothelial S1PR1signaling on brain injury after SAH, we assessed brain edema at 72 hours after induction of mild SAH by quantifying total brain water content. *S1pr1*$^{flox/flox}$ mice exhibited a statistically significant increase in brain water content in the ipsilateral hemisphere (82.83 ± 0.53%) compared to sham (81.34 ± 0.20%) (Fig. 6A). Interestingly, in *S1pr1*^{iECKO} mice, total brain edema in the ipsilateral hemisphere was significantly exacerbated (84.39 ± 0.91%) compared to *S1pr1*$^{flox/flox}$ (Fig. 6A). There were no changes in brain water content in contralateral hemisphere (SAH versus sham) in either *S1pr1*$^{flox/flox}$ *or S1pr1*^{iECKO} mice.

Next, we analyzed cell death at 24 hours after SAH using phospho-histone H2A.X (Ser 139) immunostaining, a marker for apoptosis and DNA damage [69, 70]. We found that *S1pr1*^{iECKO} mice showed significantly higher number of phospho-histone H2A.X positive cells compared to *S1pr1*$^{flox/flox}$ mice (50.85 ± 2.56% in *S1pr1*^{iECKO} versus 34.00 ± 2.98% in *S1pr1*$^{flox/flox}$) (Fig. 6B and C). No apoptotic cells were detected in sham animals.

Finally, we aimed to determine the impact of genetic deletion of S1PR1 in the endothelium on neurological outcomes after SAH. Neurological outcomes were determined by assessing motor and sensory function using a total scale of 4 to 24 (being 24 the best neurological outcome) as previously described[65, 66]. Neurological outcomes at 24h and 48h after mild SAH surgery were worsened in *S1pr1*^{iECKO} mice

514 (16.29 ± 1.37 and 17.14 ± 1.40, respectively) compared to *S1pr1*$^{flox/flox}$ mice (20.91 ±
515 0.81 and 21.00 ± 0.83, respectively) (Fig. 6D).

516 These data indicate that genetic deletion of *S1pr1* specifically in the endothelium
517 significantly exacerbates total brain edema and cell death resulting in poorer
518 neurological outcomes.

519 **Endothelial specific deletion of *S1pr1* in adult mice exacerbates blood brain**
520 **dysfunction after SAH.**

521 Given the critical role of the cerebrovascular endothelium in BBB maintenance, we
522 determined BBB dysfunction 24 hours after SAH or sham surgery. Albumin leakage was
523 quantified by Evans Blue Dye (EBD) extravasation assay, in *S1pr1*$^{flox/flox}$ and *S1pr1*^{iECKO}
524 mice. In addition, leakage of macromolecules into the brain parenchyma was
525 histologically confirmed by detection of intravenously injected 70kDa
526 tetramethylrhodamine (TMR)-dextran and immunofluorescence analysis of the
527 endothelial marker Glut-1. We found that 24 h after SAH, albumin leakage in the
528 ipsilateral hemisphere was significantly increased in *S1pr1*$^{flox/flox}$ mice compared to sham
529 animals (Fig 7A, 1.53 ± 0.06 fold in *S1pr1*$^{flox/flox}$ SAH versus *S1pr1*$^{flox/flox}$ sham) and
530 significantly higher in *S1pr1*^{iECKO} mice with regards to *S1pr1*$^{flox/flox}$ (1.83 ± 0.08 in
531 *S1pr1*^{iECKO}, Fig. 7A). In addition, upon sham surgeries, no differences in albumin leakage
532 were observed between *S1pr1*$^{flox/flox}$ and *S1pr1*^{iECKO}, consistent with our recent report
533 [56]. Histological analysis of 70kDa tetramethylrhodamine (TMR)-dextran localization,
534 confirmed increased leakage into the brain parenchyma and outside of cerebral
535 capillaries upon SAH (Fig. 7B). Altogether, these data indicate that BBB dysfunction
536 upon SAH is exacerbated in animals lacking S1PR1 specifically in the endothelium.

537 In order to shed light on the mechanisms whereby endothelial deletion of S1PR1 leads
538 to exacerbated BBB dysfunction, we isolated cerebral microvessels after SAH from

539 *S1pr1*$^{flox/flox}$ *S1pr1*^{iECKO} mice and determined the activation of signaling pathways
540 implicated in BBB dysfunction by western blot analysis. The Rho-ROCK pathway has
541 been shown to play a critical role in endothelial barrier dysfunction, endothelial
542 inflammation [77] and also in blood brain barrier dysfunction in central nervous system
543 pathologies [78-80]. We found that exacerbated BBB dysfunction in endothelial-specific
544 S1PR1 null mice correlated with increased phosphorylation of myosin light chain (MLC)
545 in isolated cortical microvessels (Fig. 7C and D, 6.96±1.6 fold in *S1pr1*^{iECKO} *versus*
546 *S1pr1*$^{flox/flox}$), a downstream effector of the Rho-ROCK pathway critical for the induction
547 blood brain barrier dysfunction [78]. The levels of endothelial markers (e.g. occludin, Fig.
548 7C and D) were similar, indicating consistent cell composition between microvessel
549 preparations [59]. Altogether, these data indicate that BBB dysfunction after SAH
550 (albumin and 70 KDa dextran leakage) is heightened in mice lacking S1PR1 specifically
551 in the endothelium and correlates with increased levels of phosphorylated MLC in
552 cerebral microvessels.
553
554

DISCUSSION

In this study, we aimed to determine the expression of S1PR1 in the cerebrovascular endothelium in mice and humans and the role of endothelial S1PR1 signaling in stroke outcomes in mice. Using tissue specific S1PR1 null mice in which genetic deletion of S1PR1 in the endothelium was induced in the adult and a mouse model of aneurysmal SAH, the most devastating type of stroke, we unveil the critical role of this endothelial pathway in SAH outcomes. We found that S1PR1 transcripts are significantly enriched (~6 fold) in mouse cortical microvessels compared to total brain and that S1PR1 mRNA is induced in cerebral microvessels after SAH. Endothelial specific deletion of S1PR1 resulted in aggravated brain injury and significantly worsened outcomes, indicating that S1PR1 is an endogenous protective mechanism of the endothelium to mitigate exacerbation of neurovascular injury in stroke. *Our study unveiled a previously unappreciated role of the endothelial S1P pathway in the pathophysiology of stroke and implies that activation of this endogenous protective endothelial pathway could have important therapeutic applications in CNS pathologies.*

Cerebral microvascular dysfunction has been implicated in the pathophysiology of numerous acute [5-13, 81] [82-85], and chronic neurological conditions [86-89]. Aneurysmal SAH, the most devastating type of stroke, occurs when an intracranial aneurysm ruptures. Compared to other types of stroke, SAH occurs earlier in life (40-60 years)[90] and leads to higher mortality (50%) [91]. In addition, SAH survivors experience a high degree of disability and cognitive impairment (memory, language and executive function) [92] with personal and societal consequences. SAH causes transient cerebral ischemia and accumulation of blood in the subarachnoid space, leading to brain injury, BBB dysfunction, cytotoxic and vasogenic cerebral edema in the acute phase [12, 93, 94]. Although numerous studies have reported *the direct correlation between*

581 *endothelial barrier dysfunction and worsened SAH outcomes in humans* [95, 96] and
582 mice [94, 97-102], *the impact of specific endothelial signaling pathways on brain injury*
583 *and SAH outcomes has remained uncertain*. Given the emerging pathophysiological
584 relevance in humans of the S1PR1 pathway, in this study, we aimed to investigate the
585 role of the endothelial-specific S1PR1 signaling in brain injury in the acute phase of
586 SAH. We used a well-established mouse model of aneurysmal SAH, the endovascular
587 rupture model [61]. This experimental model faithfully recapitulates key features of the
588 acute phase of SAH: upon rupture of the MCA, blood pours into the subarachnoid space,
589 increasing intracranial pressure which gives rise to a brief period of transient (~3-5
590 minutes) cerebral ischemia [61] (Fig. 5E, ~70%reduction of CBF in ipsilateral
591 hemisphere). CBF slowly recovers over the time, but the brain remains hypoperfused in
592 the acute phase of SAH (Fig. 5E, ~30% reduction vs basal). BBB breakdown, cerebral
593 edema and neuronal injury ensue [97, 100]. Our *study demonstrates the critical role of*
594 *the endothelium in SAH outcomes and highlights the therapeutic potential of the*
595 *endothelial S1PR1 pathway to prevent exacerbation of brain injury in this devastating*
596 *condition.*
597
598 There is mounting evidence in humans of the pathophysiological relevance of the S1P-
599 S1PR1 pathway in endothelial [31, 32] and lymphocyte function [38, 39] [40]. Fingolimod
600 [38, 39] and Siponimod [40], 2 immunosupressor drugs FDA approved for the treatment
601 of multiple sclerosis, are pharmacological modulators of S1PR1. Remarkably, they are
602 currently being tested in stroke clinical trials. In experimental stroke, FTY720 and S1PR1
603 specific agonists, as other immunosuppressor drugs, have been shown to be
604 protective[45, 46] [47, 48]. Although the mechanisms are not completely clear, FTY720
605 protection has been attributed to its immunosuppressive effects [48] and its ability to
606 desensitize and inhibit S1PR1 signaling. *Due to the immuno-suppressor effects of*

607 *S1PR1 pharmacological modulators, these previous studies could not determine the role*
608 *of endothelial specific S1PR1 signaling in BBB function and stroke outcomes*. We sought
609 to address this pivotal question by inducing the deletion of S1PR1 in adult mice,
610 specifically in the endothelium [57] and directly testing the role of endothelial S1PR1
611 signaling in BBB function and its impact on early brain injury upon SAH. Our data
612 demonstrate that *endothelial S1P signaling via S1PR1 is an endogenous protective*
613 *signaling pathway that mitigates neurovascular ischemic-hypoxic injury.* These data are
614 consistent with previous studies from our laboratory which indicated that FTY720 exerts
615 agonistic activity for S1PR1 in the endothelium and promotes endothelial barrier function
616 [17, 27]. Overall, our findings with the endothelial-specific S1PR1 mice highlight the
617 therapeutic potential of this endothelial pathway in stroke. *Future strategies to activate*
618 *this pathway specifically in the endothelium without compromising the immune response*
619 *hold promise as novel vasoprotective therapeutic agents in stroke.*
620
621 Mechanistically, we found that endothelial deletion of S1PR1 exacerbates BBB
622 dysfunction (albumin and 70kDa dextran leakage) upon SAH. BBB dysfunction
623 heightens neurovascular injury by various mechanisms such as by allowing the entrance
624 of neurotoxic plasma components into the brain parenchyma (e.g. albumin [103],
625 fibrinogen [104]) and by compromising the ability of cerebral capillaries to deliver oxygen
626 and nutrients to the neurons [7-9, 105]. In homeostatic conditions, the cerebrovascular
627 endothelium, in cooperation with pericytes and astrocytes maintain a physical, metabolic
628 and transport barrier to restrict the passage of molecules into the brain parenchyma [4,
629 106, 107]. Crosstalk between the cellular components of the blood brain barrier are
630 critical to maintain the unique phenotype of the cerebrovascular endothelium,
631 characterized by the presence of TJ as well as low expression of molecules involved in
632 vesicular trafficking (e.g. plasmalemma vesicle-associated protein) [108] [3] [109] and

633 leukocyte adhesion (e.g. ICAM-1), which prevents trafficking of plasma molecules and
634 blood cells via paracellular and transcellular routes. Upon ischemic or hypoxic injury,
635 BBB dysfunction ensues, primarily due to two cellular mechanisms, transcellular and
636 paracellular permeability. Gelatinase activity in cerebral microvessels [94, 100, 101, 110-
637 113] is induced leading to basal lamina degradation [7, 114], weakening of pericyte-
638 endothelial interactions and increased endothelial transcytosis (transcellular
639 permeability)[3, 109]. Intercellular junctions (tight and adherens junctions) [78, 115]
640 undergo post-translational modifications (e.g. phosphorylation) and disassembly from
641 the actin cytoskeleton [116] giving rise to increased paracellular permeability. Barrier
642 dysfunction is also accompanied by the acquisition of the cerebrovascular endothelium
643 of a pro-inflammatory phenotype, characterized by the expression of leukocyte-
644 endothelial adhesion molecules (e.g. E-Selectin, ICAM-1). The GTPase Rho, is
645 emerging as a central key regulator of these cellular processes. Rho, and its effector,
646 ROCK play a critical role in endothelial dysfunction via the regulation of the actin
647 cytoskeleton dynamics [78, 80], caveolin-mediated endothelial transcytosis [79, 117] as
648 well as the induction of pro-inflammatory gene expression via activation of nuclear factor
649 κ B[118, 119]. In the current study we found that, at the molecular level, exacerbated
650 BBB dysfunction in S1PR1 endothelial specific null mice correlated with increased levels
651 of phosphorylated MLC, a downstream effector of the Rho-ROCK pathway implicated in
652 blood brain barrier dysfunction [77, 78, 80]**.** Altogether, our data indicates that the
653 aggravation of albumin leakage observed in endothelial specific S1PR1 null mice
654 correlates with increased activation of Rho-ROCK pathway, implicating the role of
655 endothelial S1PR1 signaling in the regulation of the endothelial cytoskeleton and
656 vesicular trafficking leading to barrier dysfunction.
657
658 Other possible vascular mechanisms responsible for the worsened outcomes in

endothelial specific S1pr1iECKO mice vs wild type could be differences in cerebral blood flow or in bleeding upon cerebral artery rupture. However, we did not observe differences in the CBF changes or physiological parameters during and after SAH between these two groups of mice. In addition, the amount of blood in the subarachnoid space (SAH grade), which plays an important role in the severity of brain injury and SAH outcomes was similar in both groups of mice, indicating that there were no differences in bleeding or the clearance of the subarachnoid blood. Furthermore, there were no differences in hemostasis, assessed by the tail-bleeding assay, between wild type and S1pr1iECKO mice. Thus, the exacerbation of neuronal injury upon SAH in the endothelial specific s1pr1 null mice vs wild type cannot be attributed to differences in bleeding or in cerebral blood flow regulation. Altogether our data points to exacerbation of BBB permeability (albumin leakage) as the main cellular mechanism underlying the aggravation of brain injury upon endothelial deletion of S1PR1 in the adult mice, providing proof of concept of the critical role of endothelium and blood brain barrier dysfunction in SAH outcomes.

Lastly, our study also underscores the pathophysiological relevance of the S1P pathway in humans. Using RT-qPCR in combination with mouse genetic approaches and IHC techniques previously validated in our laboratory [62], we found that S1PR1 is the most abundant S1PR transcript in the mouse brain and mouse brain microvessels and widely detected in the human cerebrovascular endothelium and brain parenchyma. Our human data, together with our mouse studies using the endothelial-specific S1PR1 null mice, highlight the therapeutic and prognostic potential of the endothelial S1P pathway in stroke. Given recent human studies which indicate that S1P-S1PR1 vasoprotective signaling [28, 30] may be limiting in cardiovascular and inflammatory diseases [17, 31-34] our present data imply that patients having limiting endothelial S1PR1

antiinflammatory signaling (e.g. with lower levels of ApoM or HDL-bound S1P), could be at risk of worsened outcomes upon stroke. In addition, our data suggests that the adverse effects reported in some subsets of multiple sclerosis patients in chronic treatment with FTY720, such as macular edema or posterior reversible encephalopathy syndrome [120-123] could be due to antagonism of endothelial S1PR1.

In summary, our study demonstrates the critical role of the endothelial S1PR1 signaling in BBB function and SAH outcomes in mice. Our human data strengthen the pathophysiological relevance of these findings and highlight the therapeutic and prognostic potential of the endothelium, more specifically the endothelial S1P signaling pathway in stroke. New strategies to modulate S1P signaling specifically in the endothelium to prevent exacerbation of BBB leakage and brain injury without compromising the immune response [17, 60, 124] could hold promise as novel neurovascular protective therapies in stroke and other pathological conditions associated with BBB dysfunction [5-13, 81-85], [86-89].

ACKNOWLEDGEMENTS

This work was supported by internal funds provided by the Departments of Surgery and Emergency Medicine, BIDMC, the Department of Pathology and Laboratory Medicine, Weill Cornell Medicine, American Heart Association Grant-in-Aid 12GRNT12050110, NIH HL094465 and Leducq Foundation grants to TS. AI was partially supported by LeRoche foundation and the Tri-Institutional Therapeutics Discovery Institute.

We would like to thank Dan Li and Dr. Shou-ching Jaminet from the Multi-Gene Transcriptional Profiling Core Facility (Center for Vascular Biology Research, Beth Israel Deaconess Medical Center, Harvard Medical School) for the quantitative PCR analysis, Drs. Louise McCullough (University of Texas Health McGovern Medical School) and Tim Hla (Boston Children's Hospital) for their input in the project.

The authors declare no competing financial interests.

FIGURE LEGENDS

Figure 1. S1PR1 mRNA is the most abundant S1PR transcript in brain, brain endothelial cells and neurons and it is highly enriched in brain microvessels. S1PR mRNA levels in A) normal mouse brain, B) the mouse brain endothelial cell line bEnd.3, C) primary mouse neurons and D) primary mouse mixed glial cells. E) Comparison of S1PR1 mRNA levels in brain microvessels versus whole brain. Quantitative reverse transcription and polymerase chain reaction (RT-qPCR) demonstrates that S1PR1 transcript is predominant over the other S1PR and it is highly enriched in brain microvessels compared to whole brain. B) Log scale. The individual values and the mean ± SEM are shown. N=3-6. *$p<0.05$.

Figure 2. S1PR1 is expressed in the cerebrovascular endothelium of the mouse brain. Confocal analysis of S1PR1-eGFP fluorescence and Glut-1 immunodetection in white matter (A, corpus callosum) and grey matter (B, C, cortex) areas of the mouse brain. S1PR1-eGFP (green channel) is expressed in the cerebrovascular endothelium. Immunofluorescence for Glut-1 (endothelial marker) is shown in the red channel. C) Inset shown in panel (digital zoom). Representative pictures are shown. Scale bar 20μm. N=5-6. Sections were captured using an FluoView FV10i confocal microscope (Olympus, Japan) (original magnification, x 60). Arrows in the green channel point to bright green signal in the microvessels (Glut1 positive).

Figure 3. S1PR1 is detected in the human cerebrovascular endothelium. Representative images of S1PR1 immunohistochemistry from 5 human brain autopsy samples. Formalin-fixed paraffin-embedded tissue sections were used for immunohistochemical staining of S1PR1, as described in the Methods section. A) Expression of S1PR1 in frontal cortex grey matter (GM) and subcortical white matter (WM). Scale bar 500 μM. B) Representative picture showing S1PR1 immunopositivity in

arterioles and capillaries as well as the neuropil of the cortical grey matter. C) Detection of S1PR1 in the cerebrovascular endothelium of pial vessels. D-F) Representative pictures of S1PR1 immunodetection in the subcortical white matter. Notice S1PR1 positivity in parenchymal arterioles (D, F), venules (E) and capillaries (E, F). B-F) Scale bar 50 μM. Pictures were taken with a 60x objective (Olympus, Japan).

Figure 4. Endothelial S1PR1 is an endogenous protective pathway induced in cerebral microvessels after SAH. A-E) S1pr1, Gfap, Tjp-1 (ZO-1), Anpep (CD13) and Aqp4 mRNA levels in cerebral microvessels were quantified by RT-qPCR in sham animals 24 h after SAH. S1pr1 and Gfap are induced in cerebral microvessels after SAH. The mRNA levels of the endothelial (ZO-1, Tjp-1), pericyte (Anpep, CD13) or astrocyte (Aqp4) markers did not significantly change suggesting similar cell composition among the microvessel preparations from these groups of mice. F) Efficiency of deletion of S1PR1 in the cerebrovascular endothelium. *S1pr1*$^{flox/flox}$ and *S1pr1*^{iECKO} mice were treated with tamoxifen (75 mg kg^{-1}) for the consecutive 3 days at the age of 8 weeks. *S1pr1* mRNA levels were analyzed by qPCR in brain endothelial cells isolated from *S1pr1*$^{flox/flox}$ and *S1pr1*^{iECKO} mice, 2 weeks after tamoxifen treatment (n = 4). Efficiency of deletion in the cerebrovascular endothelium in *S1pr1*^{iECKO} mice is shown relative to *S1pr1*$^{flox/flox}$ mice. Individual values and mean ± SEM are shown. *P < 0.05, **P < 0.01, ***P < 0.001, Student's t-test. G) Survival curves in *S1pr1*$^{flox/flox}$ and *S1pr1*^{iECKO} mice after severe SAH surgery (n = 10). H) Survival curves in *S1pr1*$^{flox/flox}$ and *S1pr1*^{iECKO} mice after mild SAH surgery (n = 13 or 19). G and H) Log-rank test, *P < 0.05. Red line, *S1pr1*^{iECKO}; blue line, *S1pr1*$^{flox/flox}$.

Figure 5. Genetic deletion of *S1pr1* in the endothelium has no effect on subarachnoid blood volume, hemostasis or CBF changes after SAH.

A) Representative images of the ventral side of the brain from *S1pr1*$^{flox/flox}$ and *S1pr1*^{iECKO} mice at 24 hours after SAH. B) Subarachnoid blood volume (SAH grade) was calculated

765 by quantifying the blood in the subarachnoid space by image analysis as described in
766 methods section. (*n* = 6). (C-D) Quantification of hemostasis in the tail bleeding assay.
767 C) bleeding time and D) blood volume (*n* = 8). (B-D) Student's t-test. Individual values
768 and mean±SEM are shown. (E) CBF in the middle cerebral artery territory was
769 measured by Laser-speckle contrast imager in *S1pr1*$^{flox/flox}$ and *S1pr1*^{iECKO} mice before (0
770 min.), 1 min, 10 min, 2 h, 4 h, 24 h after SAH induction. The relative CBF values (%)
771 versus before SAH are shown. Data are mean ± SEM. (*n* = 6). Two-way ANOVA
772 followed by Bonferoni's test showed no statistically significant differences between wild
773 type and *S1PR1*^{iECKO}. Red solid line, *S1PR1*$^{flox/flox}$ ipsilateral side; blue solid, *S1PR1*^{iECKO}
774 ipsilateral; light dotted line, *S1PR1*$^{flox/flox}$ contralateral; light blue dotted line, *S1PR1*^{iECKO}
775 contralateral. IL, ipsilateral side. CL, contralateral side.
776
777 **Figure 6. Exacerbated cerebral edema and neuronal injury after SAH in endothelial**
778 **specific S1pr1 null mice** A) 72 hours after SAH, brain edema was evaluated by
779 quantification of brain water content in *S1pr1*$^{flox/flox}$ and *S1pr1*^{iECKO} mice (*n* = 7 - 14). Brain
780 water content in the ipsilateral and contralateral hemispheres was calculated as ([wet
781 weight-dry weight]/wet weight) x 100. * p<0.05, one-way ANOVA followed by Tukey's
782 test. B) Immunofluorescence confocal analysis of phospho-histone H2A.X, a marker for
783 DNA damage (green channel). Nuclear staining (DAPI) is shown in the blue channel.
784 Representative images of ipsilateral hemisphere (cortex) from *S1pr1*$^{flox/flox}$ and *S1pr1*^{iECKO}
785 mice after SAH stained are shown. Scale bar, 50 µm. C) Quantification of phospho-
786 histone H2A.X positive cells (%) (n = 7-8 mice). *P < 0.05, student's t-test. The individual
787 values and the mean ± SEM are shown. Each data point represents a mouse and it is
788 the average of 3 different fields. D) Neurological (sensory and motor) deficits after mild
789 SAH surgery in *S1pr1*$^{flox/flox}$ and *S1pr1*^{iECKO} mice (n = 12 or 14) were assessed as
790 described in methods. From 4 to 24 points: 24 points (best), 4 points (worst). Data are

mean ± SEM. *P < 0.05, **P < 0.01, One-way ANOVA followed by Tukey's test. Red line, *S1pr1*^{iECKO}; Blue line, *S1pr1*$^{flox/flox}$.

Figure 7. Endothelial specific S1pr1 null mice exhibit exacerbated BBB leakage after SAH compared to wild type littermates. A) Albumin BBB leakage, assessed by Evans Blue Dye extravasation, 24 hours after sham or SAH surgery in *S1pr1*$^{flox/flox}$ and *S1pr1*^{iECKO} mice (n = 6 - 10). Evans blue dye was circulating for 3 hours. The individual values and mean ± SEM are shown. *P < 0.05, **P < 0.01, ***P < 0.001, ****P < 0.0001 (One-way ANOVA followed by Tukey's test). y axis shows relative fluorescence units (R.F.U.) per gram of tissue. B) Histological determination of 70kDa of TMR-dextran leakage (red channel) into the brain parenchyma. Immunofluorescence for Glut-1 (endothelial marker) is shown in the green channel. Nuclear stain (DAPI) is shown in the blue channel. White arrows point to extravascular-parenchymal TMR-dextran. Representative pictures are shown. Scale bar 20μm. N=5-6. Sections were captured using an FluoView FV10i confocal microscope and a 60x objective (Olympus, Japan). C-D) Increased levels of phosphorylated myosin light chain (p-MLC) in isolated cortical microvessels in *S1pr1*^{iECKO} mice compared to *S1pr1*$^{flox/flox}$. Cortical microvessels were isolated 24 h after SAH in *S1pr1*^{iECKO} and *S1pr1*$^{flox/flox}$ mice. C) Western blot analysis for phospho-MLC (p-MLC), occludin and β-actin. D) Western blot quantification was conducted using Image J. Individual values and mean ± SEM are shown. *P < 0.05 (t test).

Table 1. Physiological variables in *S1pr1*$^{flox/flox}$ and *S1pr1*^{iECKO} mice.

Time points	Parameters	*S1pr1*$^{flox/flox}$	*S1pr1*^{iECKO}
5 min before SAH	Arterial O_2 saturation (SpO_2, %)	98.6 ± 0.2	98.4 ± 0.1
	Heart rate (b.p.m.)	442.0 ± 23.2	459.2 ± 10.7
	Pulse distention (μm)	13.8 ± 0.7	12.8 ± 0.9
	Respiratory rate (br.p.m.)	162.3 ± 4.9	155.0 ± 6.7
5 min after SAH	Arterial O_2 saturation (SpO_2, %)	98.6 ± 0.1	98.6 ± 0.2
	Heart rate (b.p.m.)	539.8 ± 9.9	549.7 ± 9.9
	Pulse distention (μm)	13.2 ± 1.1	12.5 ± 0.9
	Respiratory rate (br.p.m.)	133.3 ± 4.4	126.8 ± 6.5

bpm, beats per minute; br.p.m., breaths per minute. Pulse distention is a surrogate for pulse pressure. No significant differences were observed in the physiological parameters (arterial O_2 saturation, heart rate, pulse distention and respiratory rate) between *S1pr1*$^{flox/flox}$ and *S1pr1*^{iECKO} mice, before and after SAH

SUPPLEMENTARY FIGURE LEGENDS

Supplementary Figure 1. Expression of S1PR1-eGFP and Nissl stain in brain in the S1PR1-eGFP knock in mouse. S1PR1-eGFP fluorescence confocal analysis in grey matter (A, cortex and B, hippocampus) and white matter areas (C, corpus callosum) of the mouse brain. Neuronal somas are stained with NeuroTrace® 530/615 Red Fluorescent Nissl (red channel). Note that S1PR1-eGFP is expressed in neurons and localized around the soma, mainly in the neuropil (A, B) and axons (C). Sections were imaged by using an FluoView FV10i confocal microscope (Olympus, Japan), (original magnification, x 60). Scale bar 20μm. Representative pictures are shown. N=5-6

Supplementary Figure 2. Expression of S1PR1-eGFP and MAP-2 immunofluorescence in neurons in the S1PR1-eGFP knock in mice. S1PR1-eGFP fluorescence confocal analysis in grey matter (A, cortex and B, hippocampus) and white matter areas (C, D, internal capsule) of the mouse brain. Notice that S1PR1-eGFP signal is localized in the dendrites and neuronal processes (MAP-2 positive). D) Inset shown in panel C (digital zoom). Image shows localization of S1PR1-eGFP around the microtubules. Sections were imaged by using an FluoView FV10i confocal microscope (Olympus, Japan), (original magnification, x 60). Scale bar 20μm. Representative pictures are shown. N=5-6

Supplementary Figure 3. Expression of S1PR1-eGFP and GFAP immunofluorescence in astrocytes in the S1PR1-eGFP knock in mice. S1PR1-eGFP fluorescence confocal analysis in white matter areas (A, B, corpus callosum, C, internal capsule) of the mouse brain. Arrows indicate fibrous astrocytes positive for S1PR1-eGFP. B) Digital zoomed image of an astrocyte positive for S1PR1-eGFP. C) Digital zoomed image of an astrocyte negative for S1PR1-eGFP.Sections were imaged

by using an FluoView FV10i confocal microscope and a 60x objective (Olympus, Japan) Scale bar 20μm. Representative pictures are shown. N=5-6

Supplementary Figure 4. S1PR1 protein levels in cortical microvessels are increased 24h after SAH. Western blot analysis for S1PR1 in brain microvessels. 24 after subarachnoid hemorrhage (SAH) cortical microvessels were isolated and S1PR1 levels were detected by western blot (*n* = 4). Immunoblot image (A) and quantification of S1PR1 (B) are shown. βactin bands are used as a loading control and for normalization in quantification. Individual values and mean ±SEM are shown. ***P* < 0.01, t test.

849

Table 2. Sequences of the primers used for RT-qPCR

Target Genes	Primer's Sequences
Mouse S1PR1	F: CCGGATCGTATCTTGTTGCA R: AAATTCCATGCCTGGGATGA
Mouse S1PR2	F: ATGGGCGGCTTATACTCAGAG R: GCGCAGCACAAGATGATGAT
Mouse S1PR3	F: GCCTAGCGGGAGAGAAACCT R: CCGACTGCGGGAAGAGTGT
Mouse S1PR4	F: TTAGAGTGGTCCGAGCCAATG R: GATCATCAGCACGGTGTTGAGT
Mouse S1PR5	F: CACCGGCAGTCCTGGAGTA R: AAGGGTTGGGAAGCGTCAGT
18S	F: ACCTCTCGAAGTGTTGGATACAG R: TTCACTAATGACACAAACGTGATTC

850
851
852

REFERENCES

[1] E.J. Benjamin, S.S. Virani, C.W. Callaway, A.M. Chamberlain, A.R. Chang, S. Cheng, S.E. Chiuve, M. Cushman, F.N. Delling, R. Deo, S.D. de Ferranti, J.F. Ferguson, M. Fornage, C. Gillespie, C.R. Isasi, M.C. Jimenez, L.C. Jordan, S.E. Judd, D. Lackland, J.H. Lichtman, L. Lisabeth, S. Liu, C.T. Longenecker, P.L. Lutsey, J.S. Mackey, D.B. Matchar, K. Matsushita, M.E. Mussolino, K. Nasir, M. O'Flaherty, L.P. Palaniappan, A. Pandey, D.K. Pandey, M.J. Reeves, M.D. Ritchey, C.J. Rodriguez, G.A. Roth, W.D. Rosamond, U.K.A. Sampson, G.M. Satou, S.H. Shah, N.L. Spartano, D.L. Tirschwell, C.W. Tsao, J.H. Voeks, J.Z. Willey, J.T. Wilkins, J.H. Wu, H.M. Alger, S.S. Wong, P. Muntner, E. American Heart Association Council on, C. Prevention Statistics, S. Stroke Statistics, Heart Disease and Stroke Statistics-2018 Update: A Report From the American Heart Association, Circulation, 137 (2018) e67-e492.

[2] R.D. Bell, E.A. Winkler, I. Singh, A.P. Sagare, R. Deane, Z. Wu, D.M. Holtzman, C. Betsholtz, A. Armulik, J. Sallstrom, B.C. Berk, B.V. Zlokovic, Apolipoprotein E controls cerebrovascular integrity via cyclophilin A, Nature, 485 (2012) 512-516.

[3] A. Armulik, G. Genove, M. Mae, M.H. Nisancioglu, E. Wallgard, C. Niaudet, L. He, J. Norlin, P. Lindblom, K. Strittmatter, B.R. Johansson, C. Betsholtz, Pericytes regulate the blood-brain barrier, Nature, 468 (2010) 557-561.

[4] N.J. Abbott, L. Ronnback, E. Hansson, Astrocyte-endothelial interactions at the blood-brain barrier, Nat Rev Neurosci, 7 (2006) 41-53.

[5] J.L. Saver, Improving reperfusion therapy for acute ischaemic stroke, J Thromb Haemost, 9 Suppl 1 (2011) 333-343.

[6] C.A. Molina, J. Alvarez-Sabin, Recanalization and reperfusion therapies for acute ischemic stroke, Cerebrovasc Dis, 27 Suppl 1 (2009) 162-167.

[7] G.F. Hamann, Y. Okada, G.J. del Zoppo, Hemorrhagic transformation and microvascular integrity during focal cerebral ischemia/reperfusion, J Cereb Blood Flow Metab, 16 (1996) 1373-1378.

[8] A. Ames, 3rd, R.L. Wright, M. Kowada, J.M. Thurston, G. Majno, Cerebral ischemia. II. The no-reflow phenomenon, Am J Pathol, 52 (1968) 437-453.

[9] G.J. del Zoppo, T. Mabuchi, Cerebral microvessel responses to focal ischemia, J Cereb Blood Flow Metab, 23 (2003) 879-894.

[10] S.B. Murthy, Y. Moradiya, J. Dawson, K.R. Lees, D.F. Hanley, W.C. Ziai, K. Butcher, S. Davis, B. Gregson, P. Lyden, S. Mayer, K. Muir, T. Steiner, Perihematomal Edema and Functional Outcomes in Intracerebral Hemorrhage, Influence of Hematoma Volume and Location, 46 (2015) 3088-3092.

[11] R.L. Macdonald, R.M. Pluta, J.H. Zhang, Cerebral vasospasm after subarachnoid hemorrhage: the emerging revolution, Nature clinical practice. Neurology, 3 (2007) 256-263.

[12] R.L. Macdonald, Delayed neurological deterioration after subarachnoid haemorrhage, Nat Rev Neurol, 10 (2014) 44-58.

[13] R.M. Pluta, J. Hansen-Schwartz, J. Dreier, P. Vajkoczy, R.L. Macdonald, S. Nishizawa, H. Kasuya, G. Wellman, E. Keller, A. Zauner, N. Dorsch, J. Clark, S. Ono, T. Kiris, P. Leroux, J.H. Zhang, Cerebral vasospasm following subarachnoid hemorrhage: time for a new world of thought, Neurol Res, 31 (2009) 151-158.

[14] G.J. del Zoppo, J.M. Hallenbeck, Advances in the Vascular Pathophysiology of Ischemic Stroke, Thrombosis Research, 98 (2000) 73-81.

[15] F.M. Faraci, Vascular protection, Stroke, 34 (2003) 327-329.

[16] W.C. Aird, Spatial and temporal dynamics of the endothelium, J Thromb Haemost, 3 (2005) 1392-1406.

[17] T. Sanchez, Sphingosine-1-Phosphate Signaling in Endothelial Disorders, Current atherosclerosis reports, 18 (2016) 31.
[18] K. Venkataraman, Y.M. Lee, J. Michaud, S. Thangada, Y. Ai, H.L. Bonkovsky, N.S. Parikh, C. Habrukowich, T. Hla, Vascular endothelium as a contributor of plasma sphingosine 1-phosphate, Circ Res, 102 (2008) 669-676.
[19] S. Fukuhara, S. Simmons, S. Kawamura, A. Inoue, Y. Orba, T. Tokudome, Y. Sunden, Y. Arai, K. Moriwaki, J. Ishida, A. Uemura, H. Kiyonari, T. Abe, A. Fukamizu, M. Hirashima, H. Sawa, J. Aoki, M. Ishii, N. Mochizuki, The sphingosine-1-phosphate transporter Spns2 expressed on endothelial cells regulates lymphocyte trafficking in mice, J Clin Invest, 122 (2012) 1416-1426.
[20] R. Pappu, S.R. Schwab, I. Cornelissen, J.P. Pereira, J.B. Regard, Y. Xu, E. Camerer, Y.W. Zheng, Y. Huang, J.G. Cyster, S.R. Coughlin, Promotion of lymphocyte egress into blood and lymph by distinct sources of sphingosine-1-phosphate, Science, 316 (2007) 295-298.
[21] N. Murata, K. Sato, J. Kon, H. Tomura, M. Yanagita, A. Kuwabara, M. Ui, F. Okajima, Interaction of sphingosine 1-phosphate with plasma components, including lipoproteins, regulates the lipid receptor-mediated actions, Biochem J, 352 Pt 3 (2000) 809-815.
[22] C. Christoffersen, H. Obinata, S.B. Kumaraswamy, S. Galvani, J. Ahnstrom, M. Sevvana, C. Egerer-Sieber, Y.A. Muller, T. Hla, L.B. Nielsen, B. Dahlback, Endothelium-protective sphingosine-1-phosphate provided by HDL-associated apolipoprotein M, Proc Natl Acad Sci U S A, 108 (2011) 9613-9618.
[23] Y. Liu, R. Wada, T. Yamashita, Y. Mi, C.X. Deng, J.P. Hobson, H.M. Rosenfeldt, V.E. Nava, S.S. Chae, M.J. Lee, C.H. Liu, T. Hla, S. Spiegel, R.L. Proia, Edg-1, the G protein-coupled receptor for sphingosine-1-phosphate, is essential for vascular maturation, J Clin Invest, 106 (2000) 951-961.
[24] M.L. Allende, T. Yamashita, R.L. Proia, G-protein-coupled receptor S1P1 acts within endothelial cells to regulate vascular maturation, Blood, 102 (2003) 3665-3667.
[25] B. Jung, H. Obinata, S. Galvani, K. Mendelson, B.S. Ding, A. Skoura, B. Kinzel, V. Brinkmann, S. Rafii, T. Evans, T. Hla, Flow-regulated endothelial S1P receptor-1 signaling sustains vascular development, Developmental cell, 23 (2012) 600-610.
[26] M.J. Lee, S. Thangada, K.P. Claffey, N. Ancellin, C.H. Liu, M. Kluk, M. Volpi, R.I. Sha'afi, T. Hla, Vascular endothelial cell adherens junction assembly and morphogenesis induced by sphingosine-1-phosphate, Cell, 99 (1999) 301-312.
[27] T. Sanchez, T. Estrada-Hernandez, J.H. Paik, M.T. Wu, K. Venkataraman, V. Brinkmann, K. Claffey, T. Hla, Phosphorylation and action of the immunomodulator FTY720 inhibits vascular endothelial cell growth factor-induced vascular permeability, J Biol Chem, 278 (2003) 47281-47290.
[28] S. Galvani, M. Sanson, V.A. Blaho, S.L. Swendeman, H. Conger, B. Dahlback, M. Kono, R.L. Proia, J.D. Smith, T. Hla, HDL-bound sphingosine 1-phosphate acts as a biased agonist for the endothelial cell receptor S1P1 to limit vascular inflammation, Science signaling, 8 (2015) ra79.
[29] T. Kimura, K. Sato, A. Kuwabara, H. Tomura, M. Ishiwara, I. Kobayashi, M. Ui, F. Okajima, Sphingosine 1-phosphate may be a major component of plasma lipoproteins responsible for the cytoprotective actions in human umbilical vein endothelial cells, J Biol Chem, 276 (2001) 31780-31785.
[30] B.A. Wilkerson, G.D. Grass, S.B. Wing, W.S. Argraves, K.M. Argraves, Sphingosine 1-phosphate (S1P) carrier-dependent regulation of endothelial barrier: high density lipoprotein (HDL)-S1P prolongs endothelial barrier enhancement as compared with albumin-S1P via effects on levels, trafficking, and signaling of S1P1, J Biol Chem, 287 (2012) 44645-44653.

[31] K. Sattler, M. Graler, P. Keul, S. Weske, C.M. Reimann, H. Jindrova, P. Kleinbongard, R. Sabbadini, M. Brocker-Preuss, R. Erbel, G. Heusch, B. Levkau, Defects of High-Density Lipoproteins in Coronary Artery Disease Caused by Low Sphingosine-1-Phosphate Content: Correction by Sphingosine-1-Phosphate-Loading, Journal of the American College of Cardiology, 66 (2015) 1470-1485.
[32] K. Sattler, I. Lehmann, M. Graler, M. Brocker-Preuss, R. Erbel, G. Heusch, B. Levkau, HDL-bound sphingosine 1-phosphate (S1P) predicts the severity of coronary artery atherosclerosis, Cellular physiology and biochemistry : international journal of experimental cellular physiology, biochemistry, and pharmacology, 34 (2014) 172-184.
[33] C. Frej, A. Linder, K.E. Happonen, F.B. Taylor, F. Lupu, B. Dahlback, Sphingosine 1-phosphate and its carrier apolipoprotein M in human sepsis and in Escherichia coli sepsis in baboons, Journal of cellular and molecular medicine, 20 (2016) 1170-1181.
[34] P. Plomgaard, R.P. Dullaart, R. de Vries, A.K. Groen, B. Dahlback, L.B. Nielsen, Apolipoprotein M predicts pre-beta-HDL formation: studies in type 2 diabetic and nondiabetic subjects, Journal of internal medicine, 266 (2009) 258-267.
[35] M. Ruiz, C. Frej, A. Holmer, L.J. Guo, S. Tran, B. Dahlback, High-Density Lipoprotein-Associated Apolipoprotein M Limits Endothelial Inflammation by Delivering Sphingosine-1-Phosphate to the Sphingosine-1-Phosphate Receptor 1, Arterioscler Thromb Vasc Biol, 37 (2017) 118-129.
[36] C. Frej, A.J. Mendez, M. Ruiz, M. Castillo, T.A. Hughes, B. Dahlback, R.B. Goldberg, A Shift in ApoM/S1P Between HDL-Particles in Women With Type 1 Diabetes Mellitus Is Associated With Impaired Anti-Inflammatory Effects of the ApoM/S1P Complex, Arterioscler Thromb Vasc Biol, 37 (2017) 1194-1205.
[37] M. Matloubian, C.G. Lo, G. Cinamon, M.J. Lesneski, Y. Xu, V. Brinkmann, M.L. Allende, R.L. Proia, J.G. Cyster, Lymphocyte egress from thymus and peripheral lymphoid organs is dependent on S1P receptor 1, Nature, 427 (2004) 355-360.
[38] V. Brinkmann, M.D. Davis, C.E. Heise, R. Albert, S. Cottens, R. Hof, C. Bruns, E. Prieschl, T. Baumruker, P. Hiestand, C.A. Foster, M. Zollinger, K.R. Lynch, The immune modulator FTY720 targets sphingosine 1-phosphate receptors, J Biol Chem, 277 (2002) 21453-21457.
[39] V. Brinkmann, A. Billich, T. Baumruker, P. Heining, R. Schmouder, G. Francis, S. Aradhye, P. Burtin, Fingolimod (FTY720): discovery and development of an oral drug to treat multiple sclerosis, Nat Rev Drug Discov, 9 (2010) 883-897.
[40] S. Pan, N.S. Gray, W. Gao, Y. Mi, Y. Fan, X. Wang, T. Tuntland, J. Che, S. Lefebvre, Y. Chen, A. Chu, K. Hinterding, A. Gardin, P. End, P. Heining, C. Bruns, N.G. Cooke, B. Nuesslein-Hildesheim, Discovery of BAF312 (Siponimod), a Potent and Selective S1P Receptor Modulator, ACS medicinal chemistry letters, 4 (2013) 333-337.
[41] K. LaMontagne, A. Littlewood-Evans, C. Schnell, T. O'Reilly, L. Wyder, T. Sanchez, B. Probst, J. Butler, A. Wood, G. Liau, E. Billy, A. Theuer, T. Hla, J. Wood, Antagonism of sphingosine-1-phosphate receptors by FTY720 inhibits angiogenesis and tumor vascularization, Cancer Res, 66 (2006) 221-231.
[42] M.L. Oo, S.H. Chang, S. Thangada, M.T. Wu, K. Rezaul, V. Blaho, S.I. Hwang, D.K. Han, T. Hla, Engagement of S1P(1)-degradative mechanisms leads to vascular leak in mice, J Clin Invest, 121 (2011) 2290-2300.
[43] P. Gergely, B. Nuesslein-Hildesheim, D. Guerini, V. Brinkmann, M. Traebert, C. Bruns, S. Pan, N.S. Gray, K. Hinterding, N.G. Cooke, A. Groenewegen, A. Vitaliti, T. Sing, O. Luttringer, J. Yang, A. Gardin, N. Wang, W.J. Crumb, Jr., M. Saltzman, M. Rosenberg, E. Wallstrom, The selective sphingosine 1-phosphate receptor modulator BAF312 redirects lymphocyte distribution and has species-specific effects on heart rate, Br J Pharmacol, 167 (2012) 1035-1047.

[44] J. Quancard, B. Bollbuck, P. Janser, D. Angst, F. Berst, P. Buehlmayer, M. Streiff, C. Beerli, V. Brinkmann, D. Guerini, Paul A. Smith, Timothy J. Seabrook, M. Traebert, K. Seuwen, R. Hersperger, C. Bruns, F. Bassilana, M. Bigaud, A Potent and Selective S1P1 Antagonist with Efficacy in Experimental Autoimmune Encephalomyelitis, Chemistry & Biology, 19 (2012) 1142-1151.

[45] Y. Hasegawa, H. Suzuki, T. Sozen, W. Rolland, J.H. Zhang, Activation of sphingosine 1-phosphate receptor-1 by FTY720 is neuroprotective after ischemic stroke in rats, Stroke, 41 (2010) 368-374.

[46] Y. Wei, M. Yemisci, H.H. Kim, L.M. Yung, H.K. Shin, S.K. Hwang, S. Guo, T. Qin, N. Alsharif, V. Brinkmann, J.K. Liao, E.H. Lo, C. Waeber, Fingolimod provides long-term protection in rodent models of cerebral ischemia, Ann Neurol, (2011).

[47] V.H. Brait, G. Tarrason, A. Gavalda, N. Godessart, A.M. Planas, Selective Sphingosine 1-Phosphate Receptor 1 Agonist Is Protective Against Ischemia/Reperfusion in Mice, Stroke, 47 (2016) 3053-3056.

[48] P. Kraft, E. Gob, M.K. Schuhmann, K. Gobel, C. Deppermann, I. Thielmann, A.M. Herrmann, K. Lorenz, M. Brede, G. Stoll, S.G. Meuth, B. Nieswandt, W. Pfeilschifter, C. Kleinschnitz, FTY720 ameliorates acute ischemic stroke in mice by reducing thrombo-inflammation but not by direct neuroprotection, Stroke, 44 (2013) 3202-3210.

[49] A. Vogelgesang, U. Grunwald, S. Langner, R. Jack, B.M. Broker, C. Kessler, A. Dressel, Analysis of lymphocyte subsets in patients with stroke and their influence on infection after stroke, Stroke, 39 (2008) 237-241.

[50] U. Dirnagl, J. Klehmet, J.S. Braun, H. Harms, C. Meisel, T. Ziemssen, K. Prass, A. Meisel, Stroke-induced immunodepression: experimental evidence and clinical relevance, Stroke, 38 (2007) 770-773.

[51] W.F. Westendorp, P.J. Nederkoorn, J.D. Vermeij, M.G. Dijkgraaf, D. van de Beek, Post-stroke infection: a systematic review and meta-analysis, BMC neurology, 11 (2011) 110.

[52] L. Ulm, H. Harms, S. Ohlraun, P. Reimnitz, A. Meisel, Impact of infections on long-term outcome after severe middle cerebral artery infarction, Journal of the Neurological Sciences, 319 (2012) 15-17.

[53] Y. Fu, J. Hao, N. Zhang, L. Ren, N. Sun, Y.J. Li, Y. Yan, D. Huang, C. Yu, F.D. Shi, Fingolimod for the treatment of intracerebral hemorrhage: a 2-arm proof-of-concept study, JAMA neurology, 71 (2014) 1092-1101.

[54] Y. Fu, N. Zhang, L. Ren, Y. Yan, N. Sun, Y.J. Li, W. Han, R. Xue, Q. Liu, J. Hao, C. Yu, F.D. Shi, Impact of an immune modulator fingolimod on acute ischemic stroke, Proc Natl Acad Sci U S A, 111 (2014) 18315-18320.

[55] Z. Zhu, Y. Fu, D. Tian, N. Sun, W. Han, G. Chang, Y. Dong, X. Xu, Q. Liu, D. Huang, F.D. Shi, Combination of an Immune Modulator Fingolimod with Alteplase in Acute Ischemic Stroke: A Pilot Trial, Circulation, (2015).

[56] K. Yanagida, C.H. Liu, G. Faraco, S. Galvani, H.K. Smith, N. Burg, J. Anrather, T. Sanchez, C. Iadecola, T. Hla, Size-selective opening of the blood-brain barrier by targeting endothelial sphingosine 1-phosphate receptor 1, Proc Natl Acad Sci U S A, 114 (2017) 4531–4536.

[57] M.E. Pitulescu, I. Schmidt, R. Benedito, R.H. Adams, Inducible gene targeting in the neonatal vasculature and analysis of retinal angiogenesis in mice, Nature protocols, 5 (2010) 1518-1534.

[58] S.M. Cahalan, P.J. Gonzalez-Cabrera, G. Sarkisyan, N. Nguyen, M.T. Schaeffer, L. Huang, A. Yeager, B. Clemons, F. Scott, H. Rosen, Actions of a picomolar short-acting S1P(1) agonist in S1P(1)-eGFP knock-in mice, Nat Chem Biol, 7 (2011) 254-256.

[59] Y. Lee, H. Uchida, H. Smith, A. Ito, T. Sanchez, The isolation and molecular characterization of cerebral microvessels, Nature protocols, (2019) doi: 10.1038/s41596-019-0212-0.
[60] G.S. Kim, L. Yang, G. Zhang, H. Zhao, M. Selim, L.D. McCullough, M.J. Kluk, T. Sanchez, Critical role of sphingosine-1-phosphate receptor-2 in the disruption of cerebrovascular integrity in experimental stroke, Nature communications, 6 (2015) 7893.
[61] H. Kamii, T. Tominaga, Filament Perforation Subarachnoid Hemorrhage: Mouse Model, Animal Models of Acute Neurological Injuries (Chen J, Xu X-M, Xu ZC, Zhang JH, editors). Humana Press, Totowa, NJ, Chapter 23 (2009) 279-286.
[62] M.J. Kluk, K.P. Ryan, B. Wang, G. Zhang, S.J. Rodig, T. Sanchez, Sphingosine-1-phosphate receptor 1 in classical Hodgkin lymphoma: assessment of expression and role in cell migration, Lab Invest, 93 (2013) 462-471.
[63] T. Sugawara, R. Ayer, V. Jadhav, J.H. Zhang, A new grading system evaluating bleeding scale in filament perforation subarachnoid hemorrhage rat model, Journal of neuroscience methods, 167 (2008) 327-334.
[64] Y. Liu, N.L. Jennings, A.M. Dart, X.J. Du, Standardizing a simpler, more sensitive and accurate tail bleeding assay in mice, World journal of experimental medicine, 2 (2012) 30-36.
[65] A. Parra, M.J. McGirt, H. Sheng, D.T. Laskowitz, R.D. Pearlstein, D.S. Warner, Mouse model of subarachnoid hemorrhage associated cerebral vasospasm: methodological analysis, Neurol Res, 24 (2002) 510-516.
[66] A.K. Vellimana, E. Milner, T.D. Azad, M.D. Harries, M.L. Zhou, J.M. Gidday, B.H. Han, G.J. Zipfel, Endothelial nitric oxide synthase mediates endogenous protection against subarachnoid hemorrhage-induced cerebral vasospasm, Stroke, 42 (2011) 776-782.
[67] M. Adachi, I. Feigin, Cerebral oedema and the water content of normal white matter, Journal of neurology, neurosurgery, and psychiatry, 29 (1966) 446-450.
[68] C. Lu, F. Zhu, Y.Y. Cho, F. Tang, T. Zykova, W.Y. Ma, A.M. Bode, Z. Dong, Cell apoptosis: requirement of H2AX in DNA ladder formation, but not for the activation of caspase-3, Mol Cell, 23 (2006) 121-132.
[69] E.P. Rogakou, C. Boon, C. Redon, W.M. Bonner, Megabase Chromatin Domains Involved in DNA Double-Strand Breaks in Vivo, The Journal of Cell Biology, 146 (1999) 905-916.
[70] A. Sharma, K. Singh, A. Almasan, Histone H2AX phosphorylation: a marker for DNA damage, Methods Mol Biol, 920 (2012) 613-626.
[71] O. Uyama, N. Okamura, M. Yanase, M. Narita, K. Kawabata, M. Sugita, Quantitative evaluation of vascular permeability in the gerbil brain after transient ischemia using Evans blue fluorescence, J Cereb Blood Flow Metab, 8 (1988) 282-284.
[72] A. Hoffmann, J. Bredno, M. Wendland, N. Derugin, P. Ohara, M. Wintermark, High and Low Molecular Weight Fluorescein Isothiocyanate (FITC)-Dextrans to Assess Blood-Brain Barrier Disruption: Technical Considerations, Translational stroke research, 2 (2011) 106-111.
[73] G. Zhang, L. Yang, G.S. Kim, K. Ryan, S. Lu, R.K. O'Donnell, K. Spokes, N. Shapiro, W.C. Aird, M.J. Kluk, K. Yano, T. Sanchez, Critical role of sphingosine-1-phosphate receptor 2 (S1PR2) in acute vascular inflammation, Blood, 122 (2013) 443-455.
[74] S.C. Shih, L.E. Smith, Quantitative multi-gene transcriptional profiling using real-time PCR with a master template, Exp Mol Pathol, 79 (2005) 14-22.
[75] R. Montesano, M.S. Pepper, U. Mohle-Steinlein, W. Risau, E.F. Wagner, L. Orci, Increased proteolytic activity is responsible for the aberrant morphogenetic behavior of endothelial cells expressing the middle T oncogene, Cell, 62 (1990) 435-445.

[76] C. Muroi, M. Fujioka, S. Marbacher, J. Fandino, E. Keller, K. Iwasaki, K. Mishima, Mouse model of subarachnoid hemorrhage: technical note on the filament perforation model, Acta Neurochir Suppl, 120 (2015) 315-320.
[77] E. Vandenbroucke, D. Mehta, R. Minshall, A.B. Malik, Regulation of endothelial junctional permeability, Ann N Y Acad Sci, 1123 (2008) 134-145.
[78] Y. Shi, L. Zhang, H. Pu, L. Mao, X. Hu, X. Jiang, N. Xu, R.A. Stetler, F. Zhang, X. Liu, R.K. Leak, R.F. Keep, X. Ji, J. Chen, Rapid endothelial cytoskeletal reorganization enables early blood–brain barrier disruption and long-term ischaemic reperfusion brain injury, Nature communications, 7 (2016) 10523.
[79] H. Sadeghian, B. Lacoste, T. Qin, X. Toussay, R. Rosa, F. Oka, D.Y. Chung, T. Takizawa, C. Gu, C. Ayata, Spreading depolarizations trigger caveolin-1–dependent endothelial transcytosis, Annals of Neurology, 84 (2018) 409-423.
[80] C.R. Kuhlmann, R. Tamaki, M. Gamerdinger, V. Lessmann, C. Behl, O.S. Kempski, H.J. Luhmann, Inhibition of the myosin light chain kinase prevents hypoxia-induced blood-brain barrier disruption, J Neurochem, 102 (2007) 501-507.
[81] D. Shlosberg, M. Benifla, D. Kaufer, A. Friedman, Blood-brain barrier breakdown as a therapeutic target in traumatic brain injury, Nat Rev Neurol, 6 (2010) 393-403.
[82] A. Chodobski, B.J. Zink, J. Szmydynger-Chodobska, Blood-brain barrier pathophysiology in traumatic brain injury, Translational stroke research, 2 (2011) 492-516.
[83] K. Kenney, F. Amyot, M. Haber, A. Pronger, T. Bogoslovsky, C. Moore, R. Diaz-Arrastia, Cerebral Vascular Injury in Traumatic Brain Injury, Experimental Neurology, 275 (2016) 353-366.
[84] A. Pitkanen, W. Loscher, A. Vezzani, A.J. Becker, M. Simonato, K. Lukasiuk, O. Grohn, J.P. Bankstahl, A. Friedman, E. Aronica, J.A. Gorter, T. Ravizza, S.M. Sisodiya, M. Kokaia, H. Beck, Advances in the development of biomarkers for epilepsy, Lancet Neurol, 15 (2016) 843-856.
[85] E. Iacobone, J. Bailly-Salin, A. Polito, D. Friedman, R.D. Stevens, T. Sharshar, Sepsis-associated encephalopathy and its differential diagnosis, Critical care medicine, 37 (2009) S331-336.
[86] D.A. Nation, M.D. Sweeney, A. Montagne, A.P. Sagare, L.M. D'Orazio, M. Pachicano, F. Sepehrband, A.R. Nelson, D.P. Buennagel, M.G. Harrington, T.L.S. Benzinger, A.M. Fagan, J.M. Ringman, L.S. Schneider, J.C. Morris, H.C. Chui, M. Law, A.W. Toga, B.V. Zlokovic, Blood-brain barrier breakdown is an early biomarker of human cognitive dysfunction, Nat Med, (2019).
[87] A. Montagne, S.R. Barnes, M.D. Sweeney, M.R. Halliday, A.P. Sagare, Z. Zhao, A.W. Toga, R.E. Jacobs, C.Y. Liu, L. Amezcua, M.G. Harrington, H.C. Chui, M. Law, B.V. Zlokovic, Blood-brain barrier breakdown in the aging human hippocampus, Neuron, 85 (2015) 296-302.
[88] B.V. Zlokovic, The blood-brain barrier in health and chronic neurodegenerative disorders, Neuron, 57 (2008) 178-201.
[89] C.P. Doherty, E. O'Keefe, E. Wallace, T. Loftus, J. Keaney, J. Kealy, M.M. Humphries, M.G. Molloy, J.F. Meaney, M. Farrell, M. Campbell, Blood-Brain Barrier Dysfunction as a Hallmark Pathology in Chronic Traumatic Encephalopathy, J Neuropathol Exp Neurol, 75 (2016) 656-662.
[90] S.C. Johnston, S. Selvin, D.R. Gress, The burden, trends, and demographics of mortality from subarachnoid hemorrhage, Neurology, 50 (1998) 1413-1418.
[91] J. van Gijn, R.S. Kerr, G.J. Rinkel, Subarachnoid haemorrhage, Lancet, 369 (2007) 306-318.
[92] T. Al-Khindi, R.L. Macdonald, T.A. Schweizer, Cognitive and functional outcome after aneurysmal subarachnoid hemorrhage, Stroke, 41 (2010) e519-536.

[93] T. Dóczi, The pathogenetic and prognostic significance of blood-brain barrier damage at the acute stage of aneurysmal subarachnoid haemorrhage. Clinical and experimental studies, Acta Neurochirurgica, 77 (1985) 110-132.
[94] S. Park, M. Yamaguchi, C. Zhou, J.W. Calvert, J. Tang, J.H. Zhang, Neurovascular protection reduces early brain injury after subarachnoid hemorrhage, Stroke, 35 (2004) 2412-2417.
[95] P. Lackner, A. Dietmann, R. Beer, M. Fischer, G. Broessner, R. Helbok, J. Marxgut, B. Pfausler, E. Schmutzhard, Cellular Microparticles as a Marker for Cerebral Vasospasm in Spontaneous Subarachnoid Hemorrhage, Stroke, 41 (2010) 2353-2357.
[96] M. Fischer, G. Broessner, A. Dietmann, R. Beer, R. Helbok, B. Pfausler, A. Chemelli, E. Schmutzhard, P. Lackner, Angiopoietin-1 is associated with cerebral vasospasm and delayed cerebral ischemia in subarachnoid hemorrhage, BMC neurology, 11 (2011) 59.
[97] H. Suzuki, Y. Hasegawa, K. Kanamaru, J.H. Zhang, Mechanisms of osteopontin-induced stabilization of blood-brain barrier disruption after subarachnoid hemorrhage in rats, Stroke, 41 (2010) 1783-1790.
[98] O. Altay, H. Suzuki, Y. Hasegawa, B. Caner, P.R. Krafft, M. Fujii, J. Tang, J.H. Zhang, Isoflurane attenuates blood-brain barrier disruption in ipsilateral hemisphere after subarachnoid hemorrhage in mice, Stroke, 43 (2012) 2513-2516.
[99] Z. Wang, C.J. Meng, X.M. Shen, Z. Shu, C. Ma, G.Q. Zhu, H.X. Liu, W.C. He, X.B. Sun, L. Huo, J. Zhang, G. Chen, Potential contribution of hypoxia-inducible factor-1alpha, aquaporin-4, and matrix metalloproteinase-9 to blood-brain barrier disruption and brain edema after experimental subarachnoid hemorrhage, Journal of molecular neuroscience : MN, 48 (2012) 273-280.
[100] Y. Egashira, H. Zhao, Y. Hua, R.F. Keep, G. Xi, White Matter Injury After Subarachnoid Hemorrhage: Role of Blood-Brain Barrier Disruption and Matrix Metalloproteinase-9, Stroke, 46 (2015) 2909-2915.
[101] F.A. Sehba, G. Mostafa, J. Knopman, V. Friedrich, Jr., J.B. Bederson, Acute alterations in microvascular basal lamina after subarachnoid hemorrhage, J Neurosurg, 101 (2004) 633-640.
[102] D.A. Siler, Y.A. Berlow, A. Kukino, C.M. Davis, J.W. Nelson, M.R. Grafe, H. Ono, J.S. Cetas, M. Pike, N.J. Alkayed, Soluble Epoxide Hydrolase in Hydrocephalus, Cerebral Edema, and Vascular Inflammation After Subarachnoid Hemorrhage, Stroke, 46 (2015) 1916-1922.
[103] I. Weissberg, L. Wood, L. Kamintsky, O. Vazquez, D.Z. Milikovsky, A. Alexander, H. Oppenheim, C. Ardizzone, A. Becker, F. Frigerio, A. Vezzani, M.S. Buckwalter, J.R. Huguenard, A. Friedman, D. Kaufer, Albumin induces excitatory synaptogenesis through astrocytic TGF-beta/ALK5 signaling in a model of acquired epilepsy following blood-brain barrier dysfunction, Neurobiol Dis, 78 (2015) 115-125.
[104] M.A. Petersen, J.K. Ryu, K. Akassoglou, Fibrinogen in neurological diseases: mechanisms, imaging and therapeutics, Nat Rev Neurosci, 19 (2018) 283-301.
[105] R.F. Keep, A.V. Andjelkovic, J. Xiang, S.M. Stamatovic, D.A. Antonetti, Y. Hua, G. Xi, Brain endothelial cell junctions after cerebral hemorrhage: Changes, mechanisms and therapeutic targets, J Cereb Blood Flow Metab, (2018) 271678X18774666.
[106] B. Obermeier, R. Daneman, R.M. Ransohoff, Development, maintenance and disruption of the blood-brain barrier, Nat Med, 19 (2013) 1584-1596.
[107] S. Liebner, R.M. Dijkhuizen, Y. Reiss, K.H. Plate, D. Agalliu, G. Constantin, Functional morphology of the blood–brain barrier in health and disease, Acta Neuropathologica, 135 (2018) 311-336.
[108] S. Nag, Morphology and molecular properties of cellular components of normal cerebral vessels, Methods in molecular medicine, 89 (2003) 3-36.

[109] R. Daneman, L. Zhou, A.A. Kebede, B.A. Barres, Pericytes are required for blood-brain barrier integrity during embryogenesis, Nature, 468 (2010) 562-566.
[110] Y. Gasche, M. Fujimura, Y. Morita-Fujimura, J.C. Copin, M. Kawase, J. Massengale, P.H. Chan, Early appearance of activated matrix metalloproteinase-9 after focal cerebral ischemia in mice: a possible role in blood-brain barrier dysfunction, J Cereb Blood Flow Metab, 19 (1999) 1020-1028.
[111] G.A. Rosenberg, E.Y. Estrada, J.E. Dencoff, Matrix metalloproteinases and TIMPs are associated with blood-brain barrier opening after reperfusion in rat brain, Stroke, 29 (1998) 2189-2195.
[112] M. Asahi, T. Sumii, M.E. Fini, S. Itohara, E.H. Lo, Matrix metalloproteinase 2 gene knockout has no effect on acute brain injury after focal ischemia, Neuroreport, 12 (2001) 3003-3007.
[113] M. Asahi, X. Wang, T. Mori, T. Sumii, J.C. Jung, M.A. Moskowitz, M.E. Fini, E.H. Lo, Effects of matrix metalloproteinase-9 gene knock-out on the proteolysis of blood-brain barrier and white matter components after cerebral ischemia, J Neurosci, 21 (2001) 7724-7732.
[114] G.F. Hamann, Y. Okada, R. Fitridge, G.J. del Zoppo, Microvascular basal lamina antigens disappear during cerebral ischemia and reperfusion, Stroke, 26 (1995) 2120-2126.
[115] D. Knowland, A. Arac, K.J. Sekiguchi, M. Hsu, S.E. Lutz, J. Perrino, G.K. Steinberg, B.A. Barres, A. Nimmerjahn, D. Agalliu, Stepwise recruitment of transcellular and paracellular pathways underlies blood-brain barrier breakdown in stroke, Neuron, 82 (2014) 603-617.
[116] D. Günzel, A.S.L. Yu, Claudins and the modulation of tight junction permeability, Physiological reviews, 93 (2013) 525-569.
[117] Z. Li, Y.H. Liu, Y.X. Xue, L.B. Liu, P. Wang, Low-dose endothelial monocyte-activating polypeptide-ii increases permeability of blood-tumor barrier by caveolae-mediated transcellular pathway, Journal of molecular neuroscience : MN, 52 (2014) 313-322.
[118] K.N. Anwar, F. Fazal, A.B. Malik, A. Rahman, RhoA/Rho-associated kinase pathway selectively regulates thrombin-induced intercellular adhesion molecule-1 expression in endothelial cells via activation of I kappa B kinase beta and phosphorylation of RelA/p65, J Immunol, 173 (2004) 6965-6972.
[119] M. Gorovoy, R. Neamu, J. Niu, S. Vogel, D. Predescu, J. Miyoshi, Y. Takai, V. Kini, D. Mehta, A.B. Malik, T. Voyno-Yasenetskaya, RhoGDI-1 modulation of the activity of monomeric RhoGTPase RhoA regulates endothelial barrier function in mouse lungs, Circ Res, 101 (2007) 50-58.
[120] L. Kappos, D.K. Li, O. Stuve, H.P. Hartung, M.S. Freedman, B. Hemmer, P. Rieckmann, X. Montalban, T. Ziemssen, B. Hunter, S. Arnould, E. Wallstrom, K. Selmaj, Safety and Efficacy of Siponimod (BAF312) in Patients With Relapsing-Remitting Multiple Sclerosis: Dose-Blinded, Randomized Extension of the Phase 2 BOLD Study, JAMA neurology, 73 (2016) 1089-1098.
[121] L. Kappos, E.W. Radue, P. O'Connor, C. Polman, R. Hohlfeld, P. Calabresi, K. Selmaj, C. Agoropoulou, M. Leyk, L. Zhang-Auberson, P. Burtin, F.S. Group, A placebo-controlled trial of oral fingolimod in relapsing multiple sclerosis, N Engl J Med, 362 (2010) 387-401.
[122] J.A. Cohen, F. Barkhof, G. Comi, H.P. Hartung, B.O. Khatri, X. Montalban, J. Pelletier, R. Capra, P. Gallo, G. Izquierdo, K. Tiel-Wilck, A. de Vera, J. Jin, T. Stites, S. Wu, S. Aradhye, L. Kappos, T.S. Group, Oral fingolimod or intramuscular interferon for relapsing multiple sclerosis, N Engl J Med, 362 (2010) 402-415.

[123] H. Linda, A. von Heijne, A case of posterior reversible encephalopathy syndrome associated with gilenya((R)) (fingolimod) treatment for multiple sclerosis, Frontiers in neurology, 6 (2015) 39.
[124] S.L. Swendeman, Y. Xiong, A. Cantalupo, H. Yuan, N. Burg, Y. Hisano, A. Cartier, C.H. Liu, E. Engelbrecht, V. Blaho, Y. Zhang, K. Yanagida, S. Galvani, H. Obinata, J.E. Salmon, T. Sanchez, A. Di Lorenzo, T. Hla, An engineered S1P chaperone attenuates hypertension and ischemic injury, Science signaling, 10 (2017).

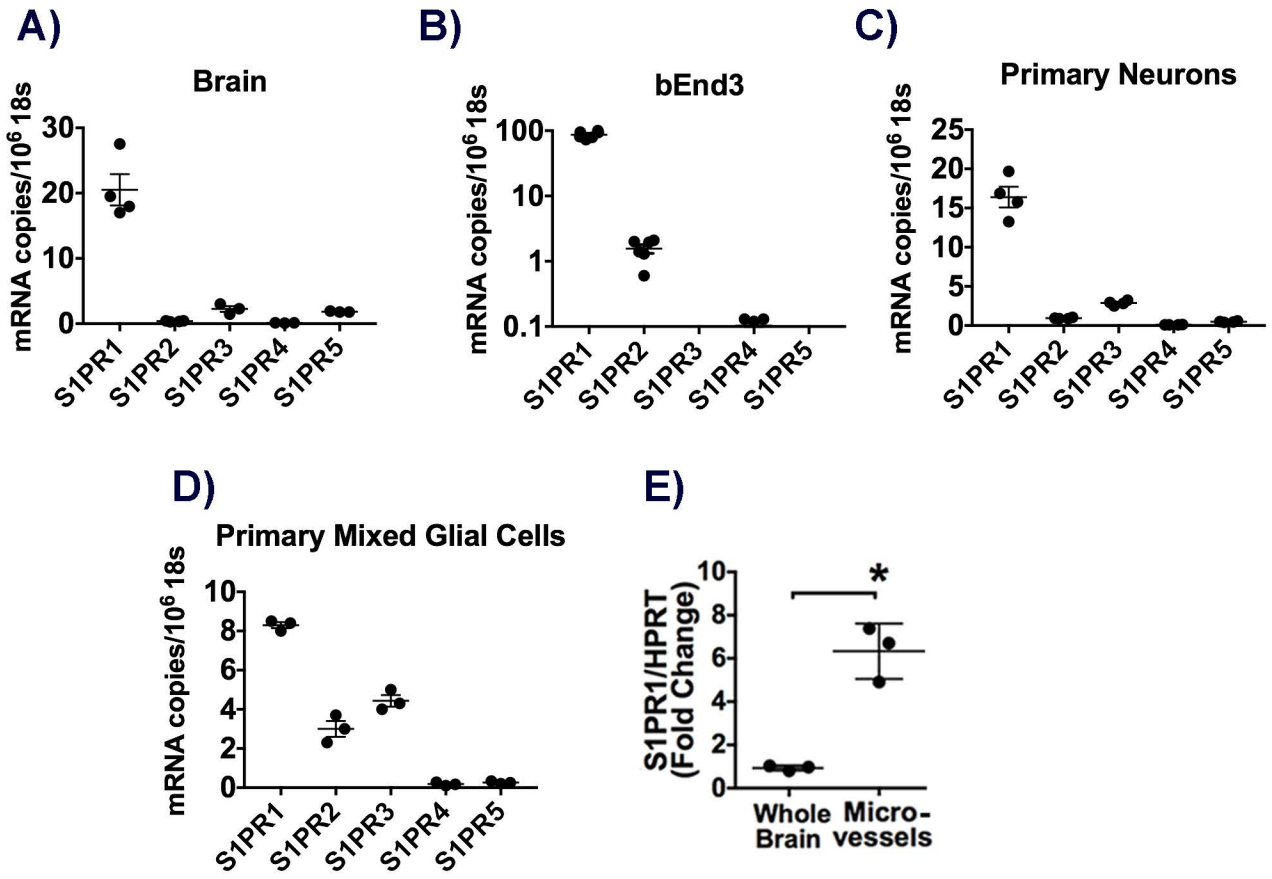

Figure 1

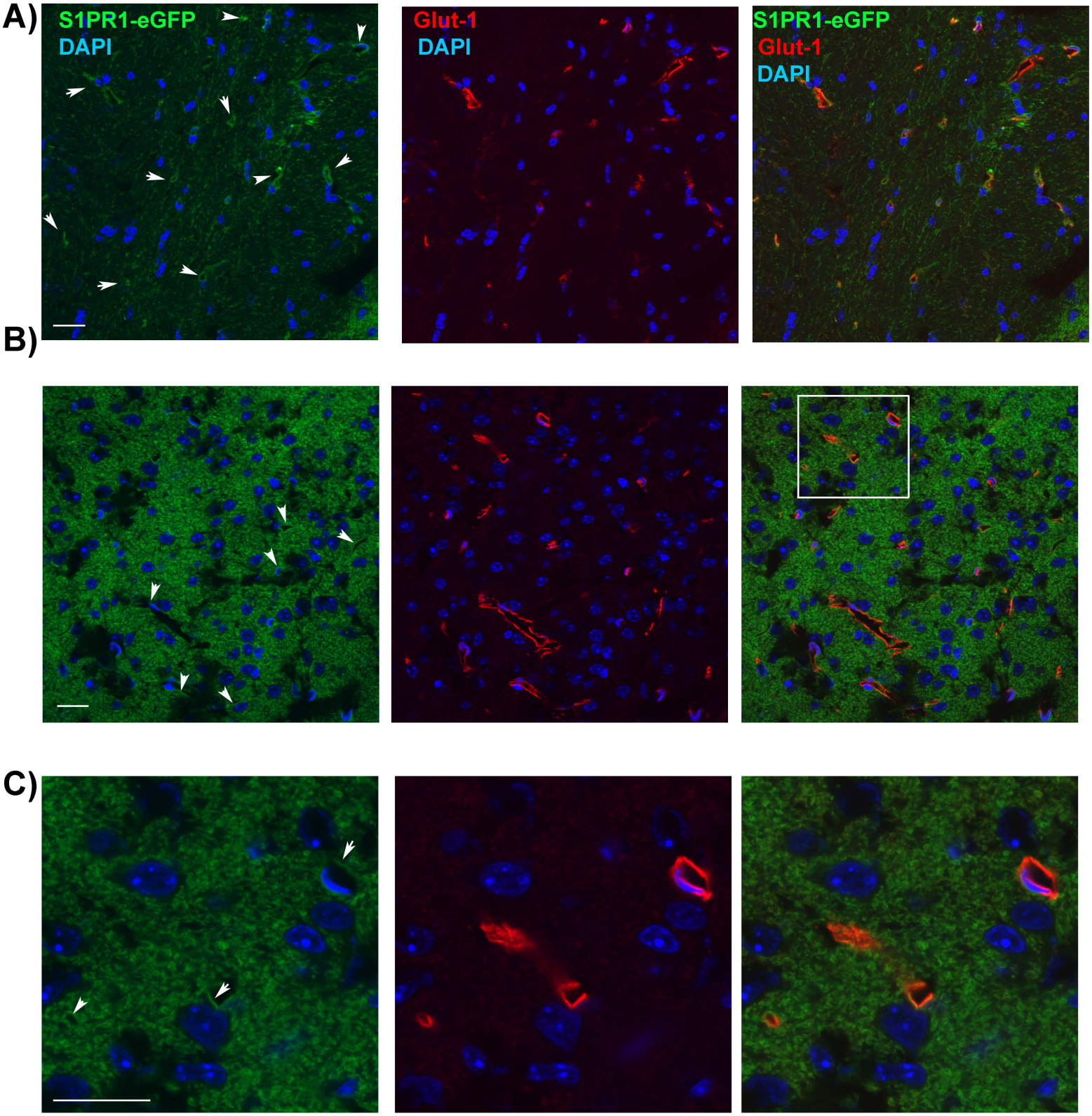

Figure 2

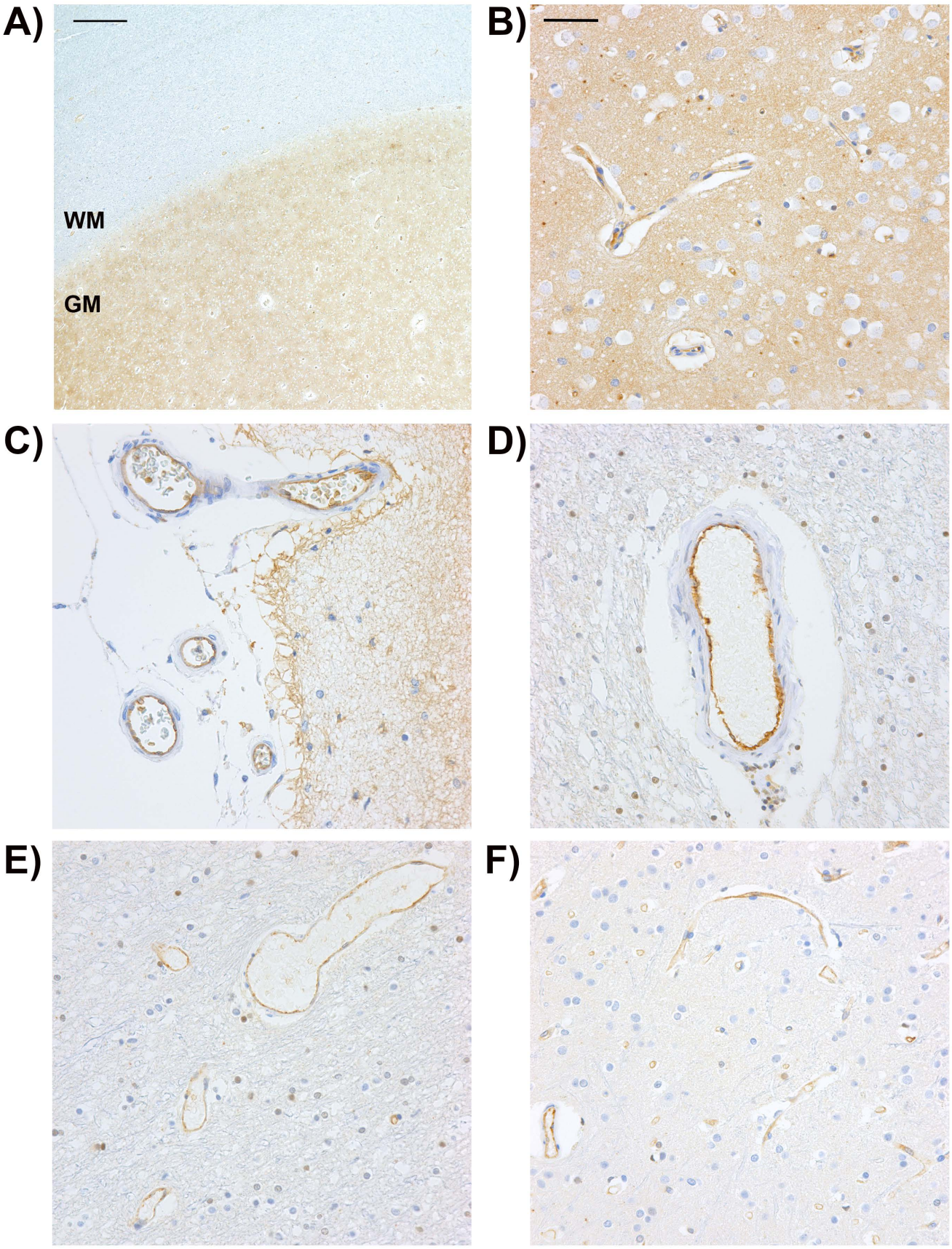

Figure 3

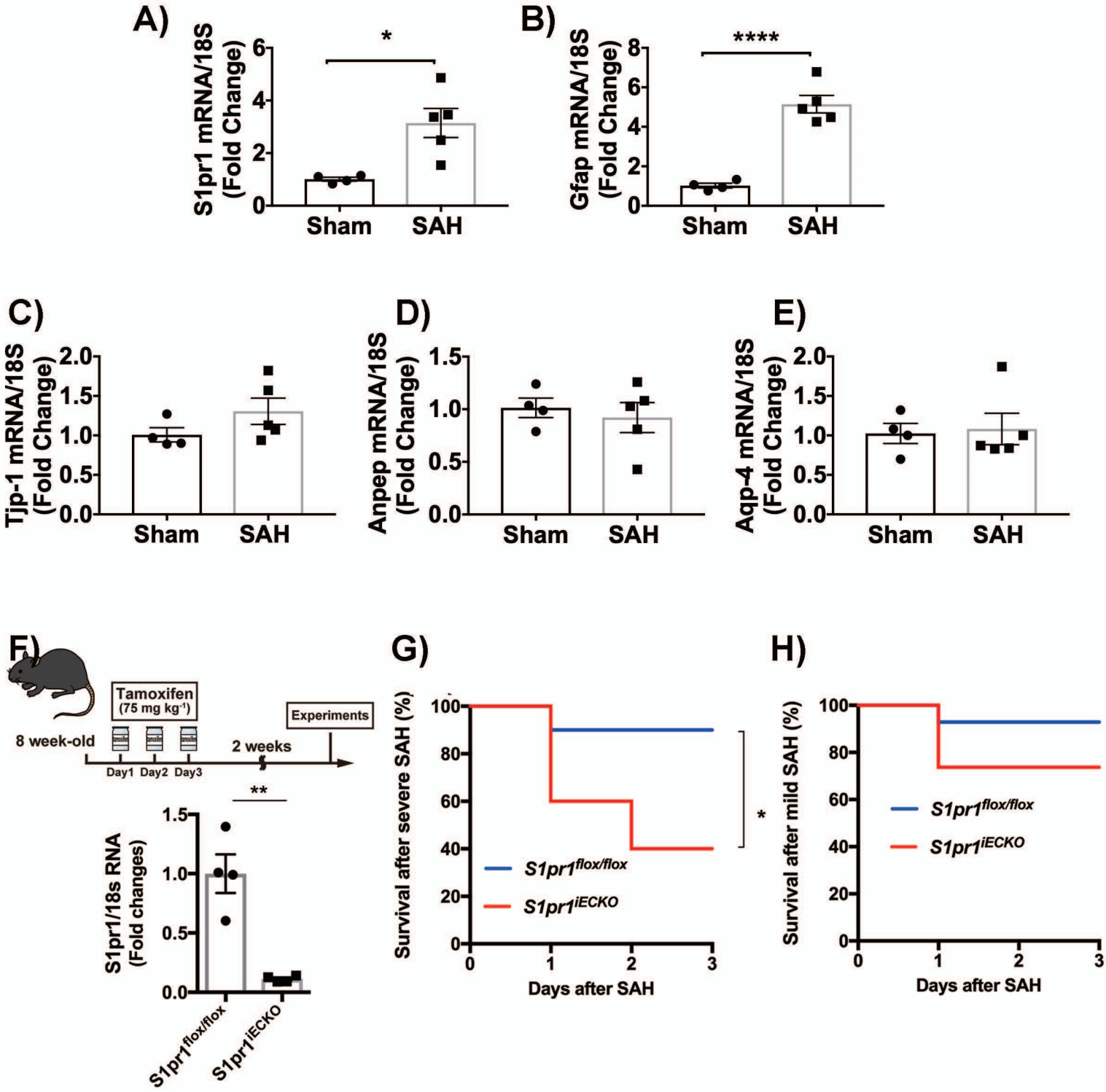

Figure 4

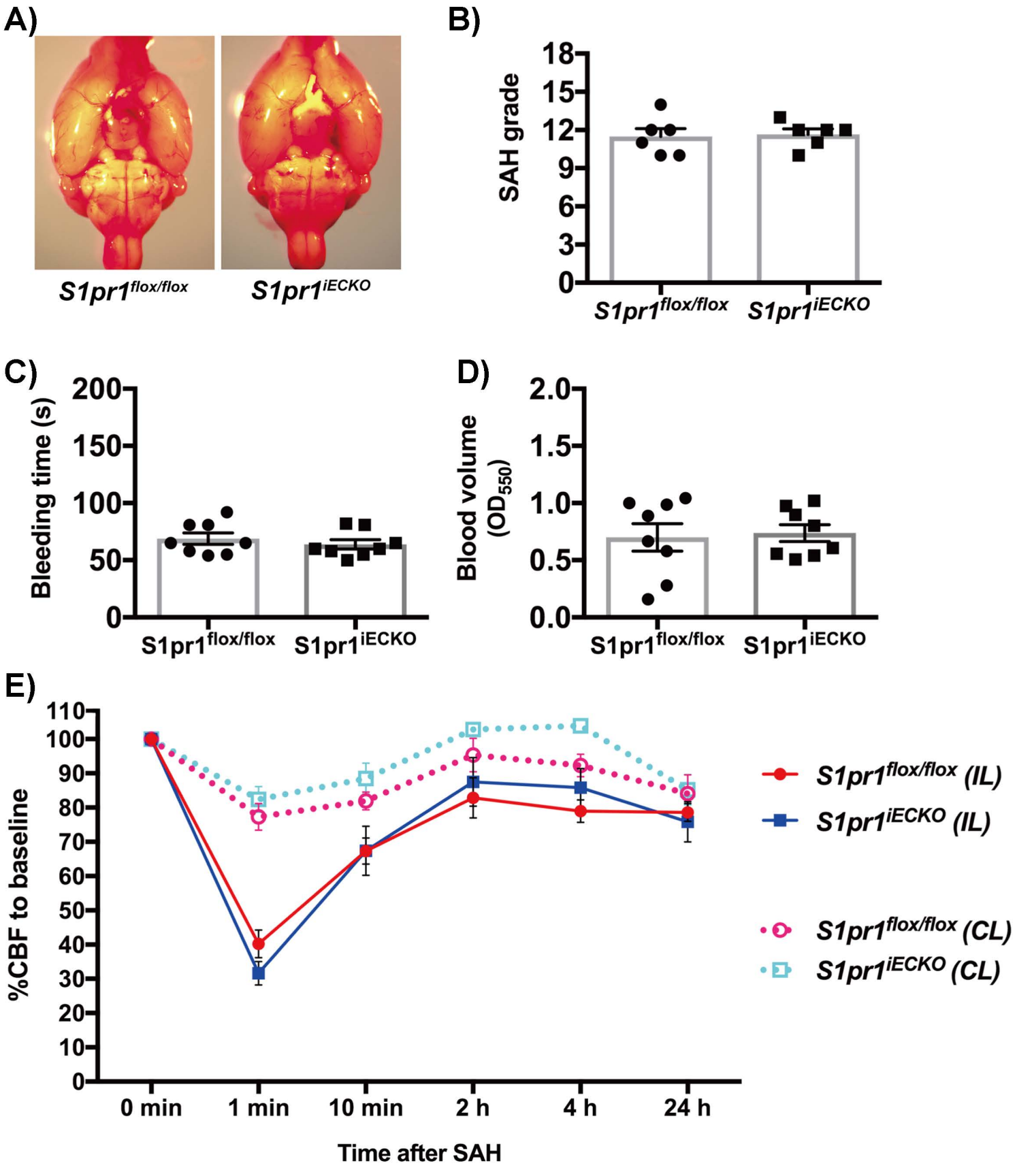

Figure 5

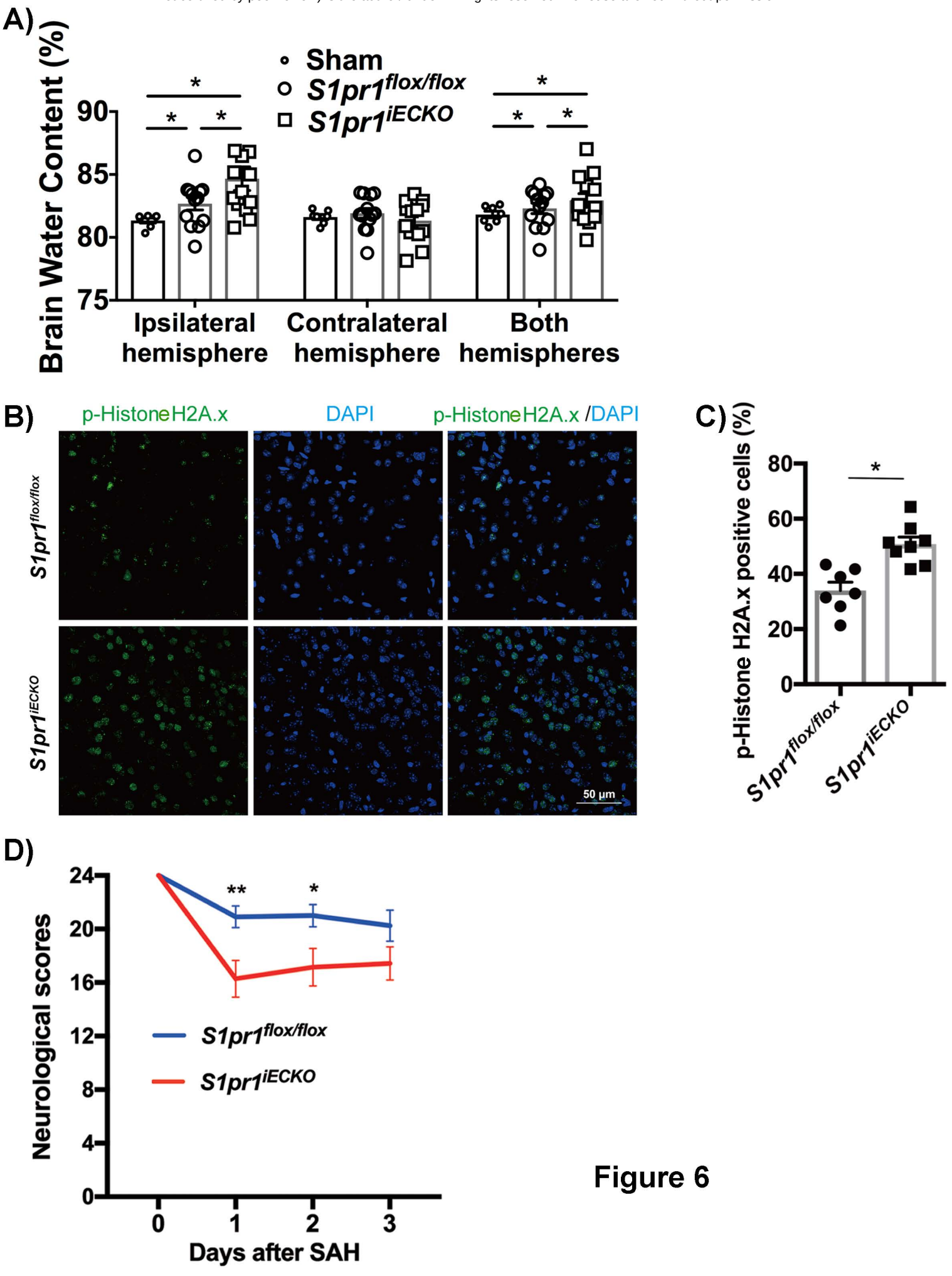

Figure 6

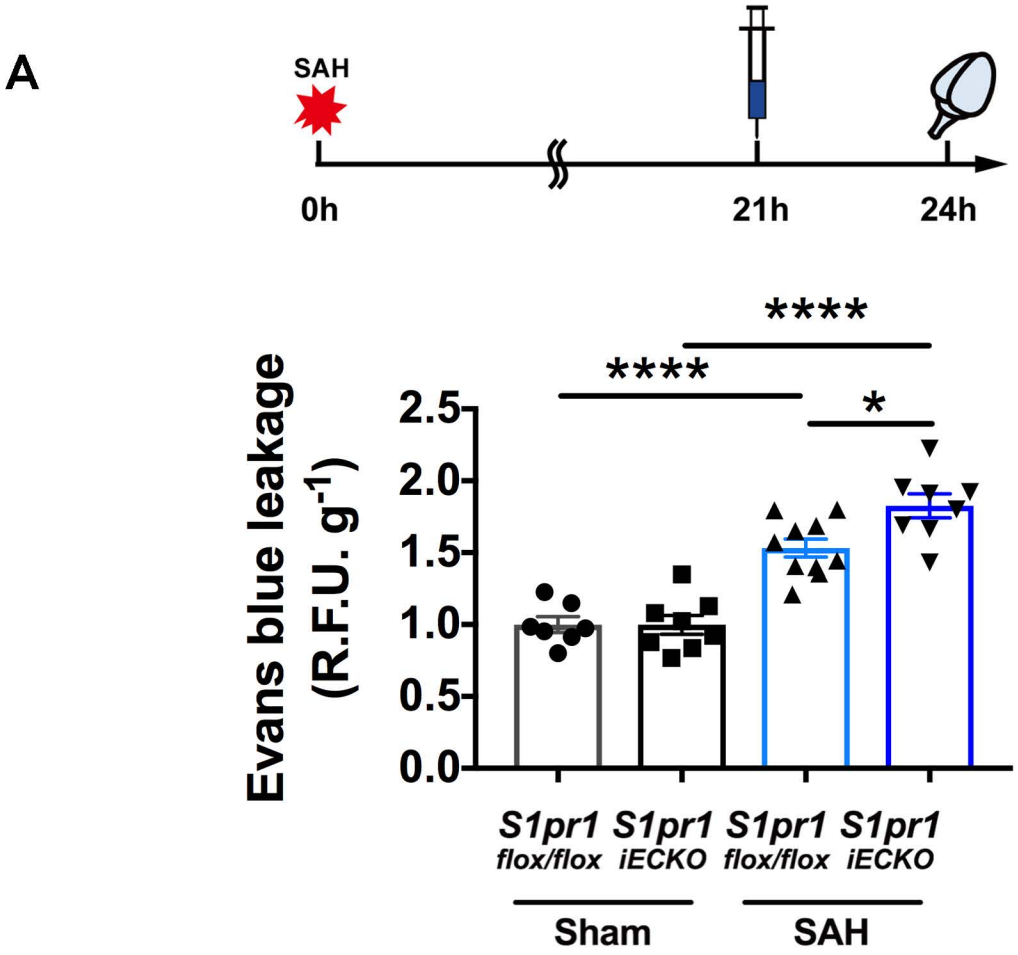

Figure 7

B

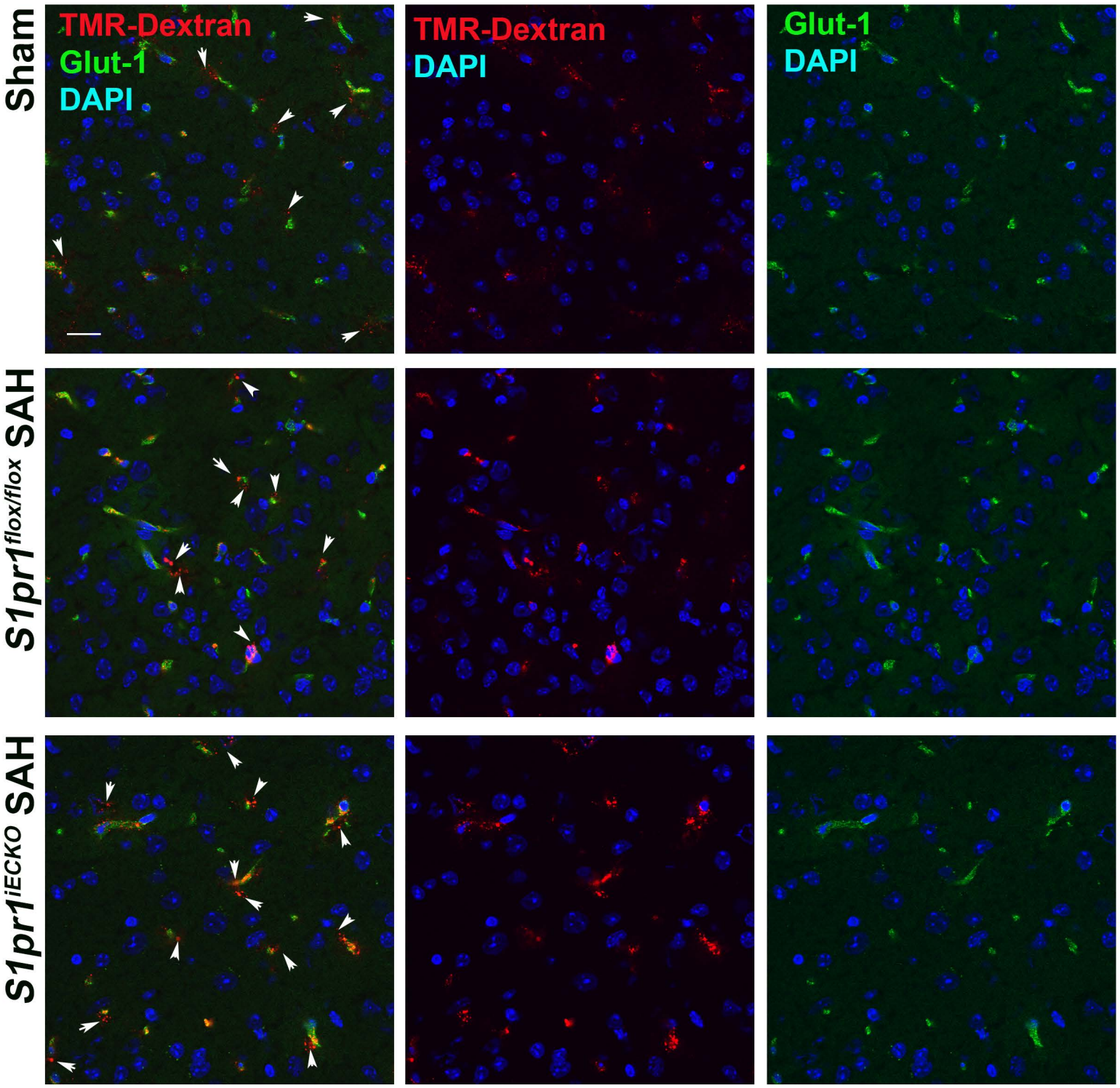

Figure 7

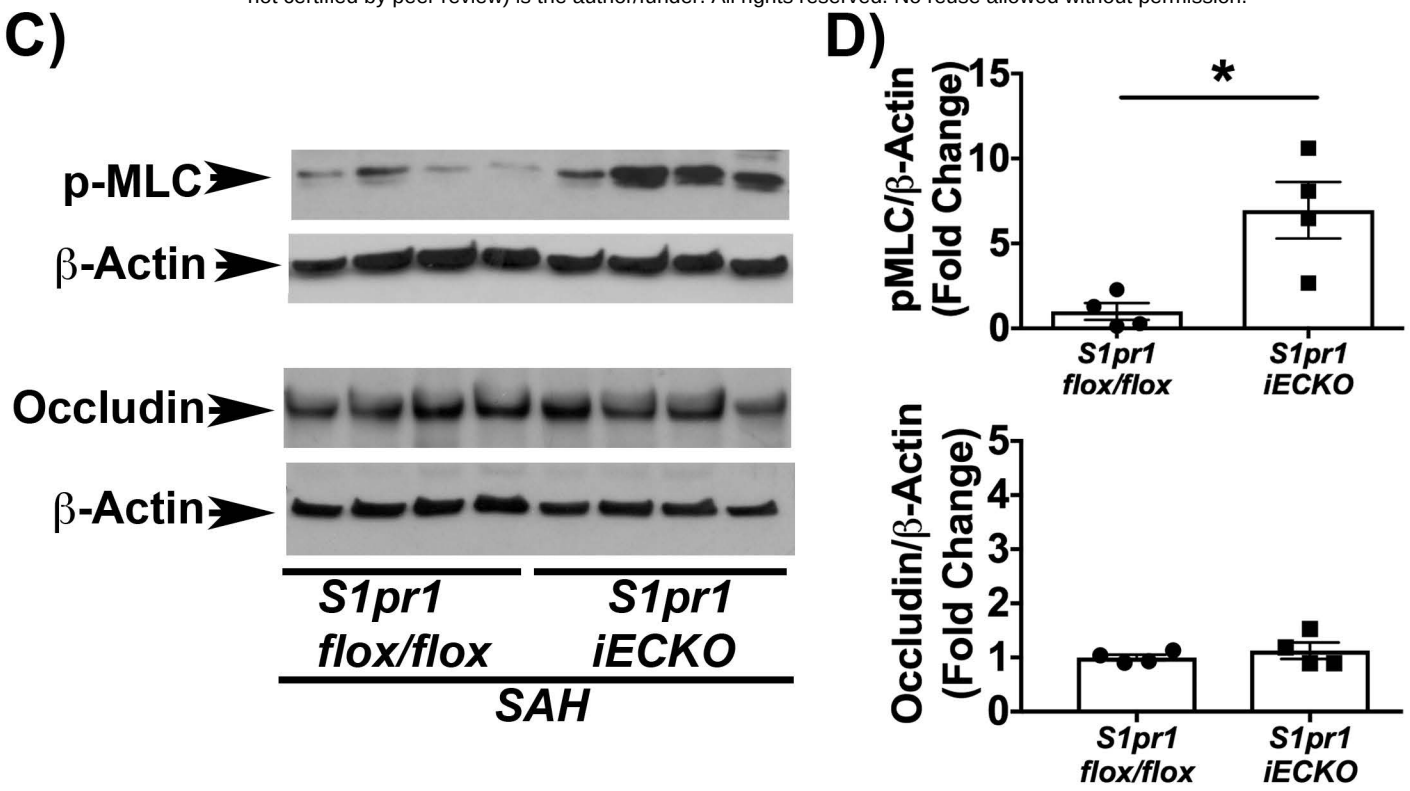

Figure 7

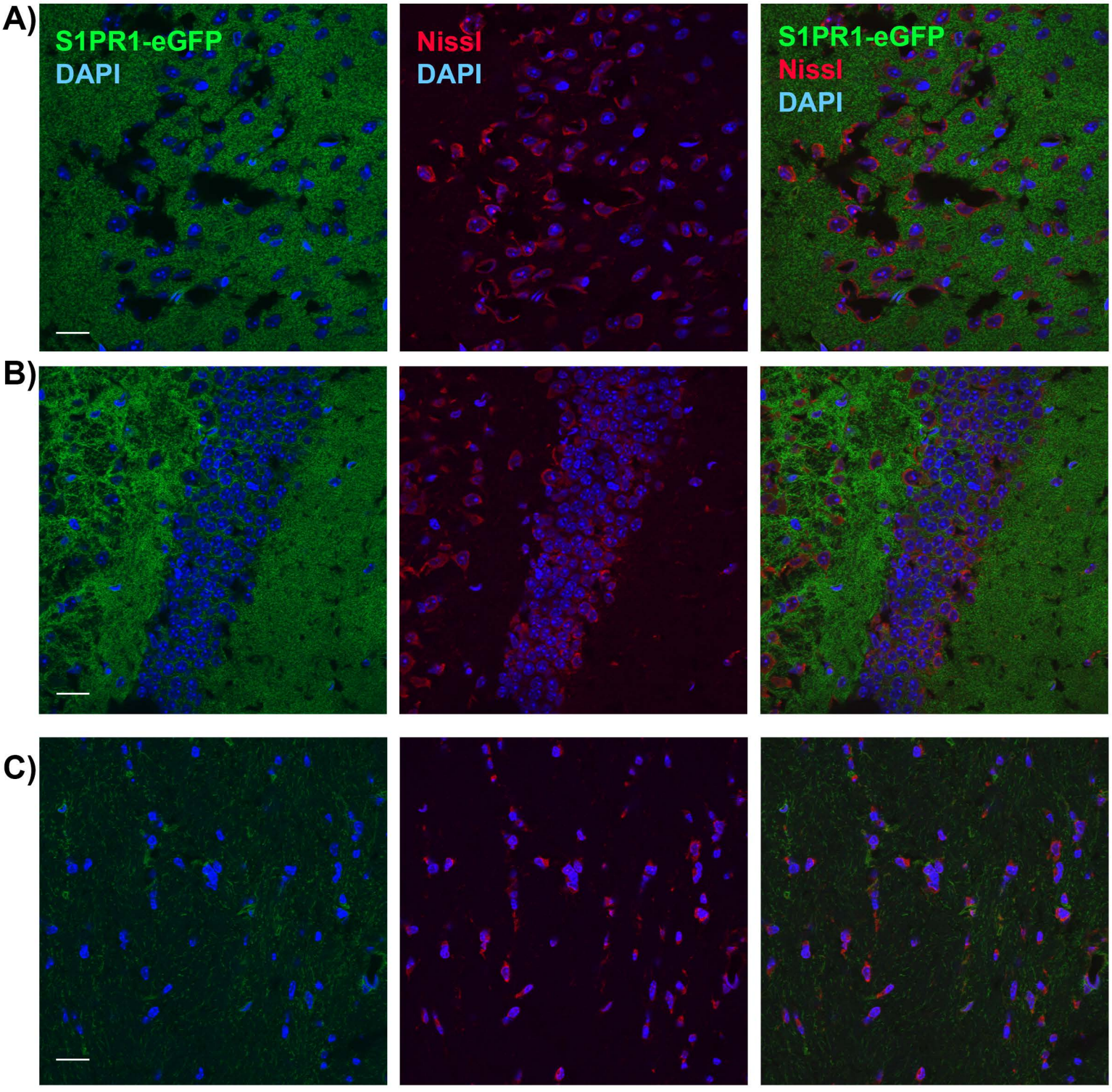

Supplementary Figure 1

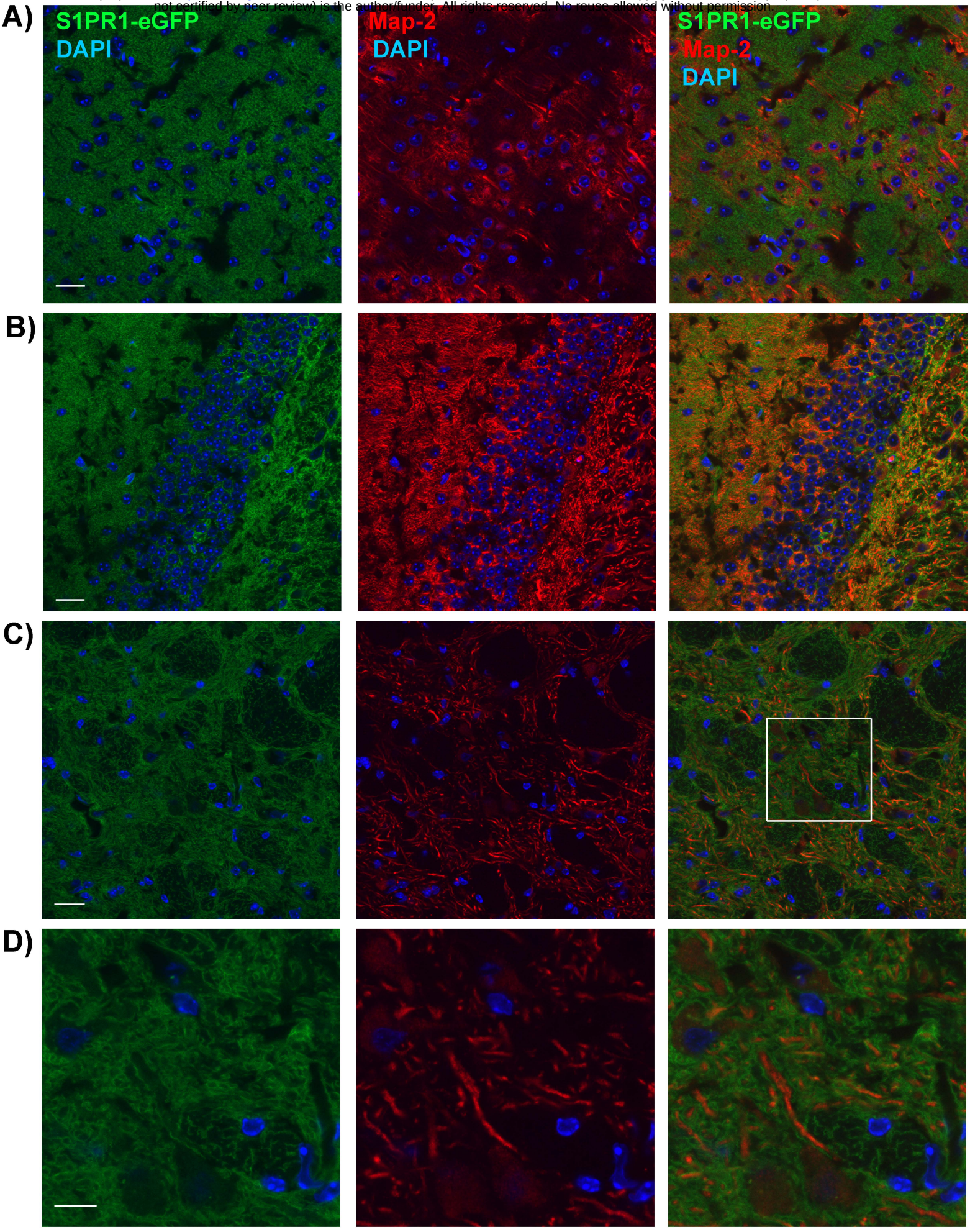

Supplementary Figure 2

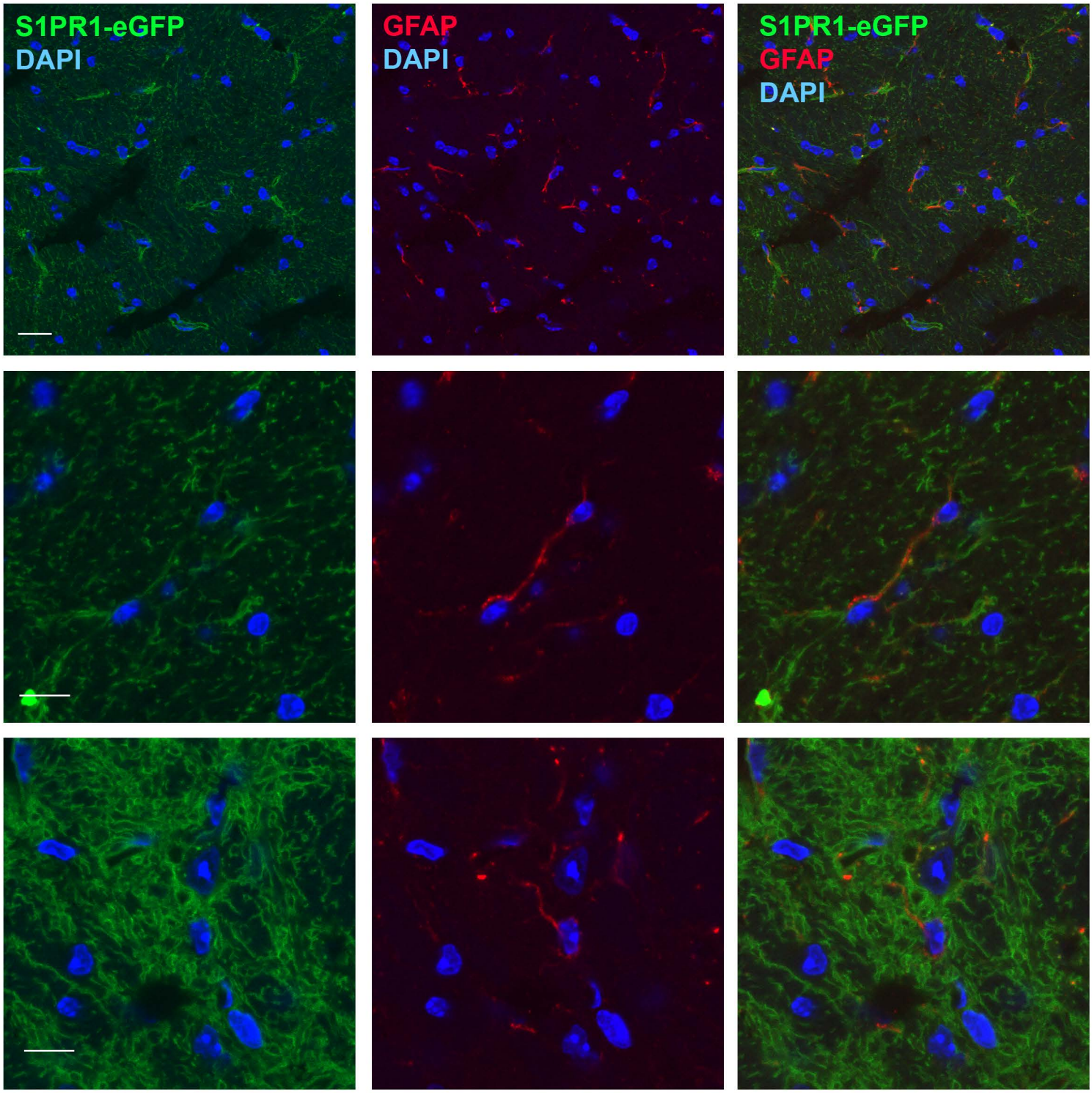

Supplementary Figure 3

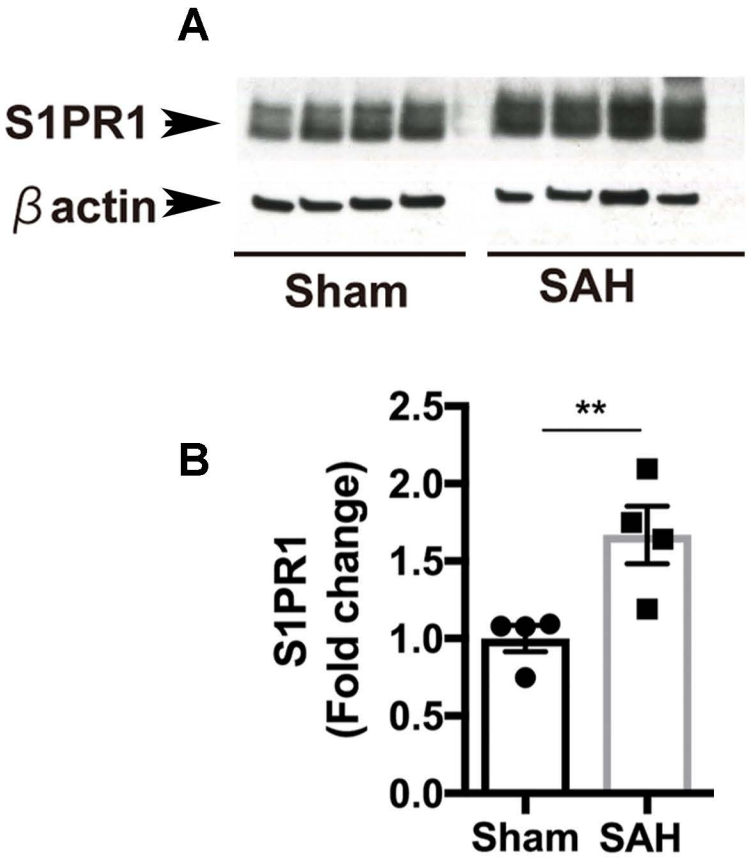

Supplementary Figure 4